

1. Report No. SWUTC/10/476660-00012-1	2. Government Accession No.	3. Recipient's Catalog No.	
4. Title and Subtitle PHYSICALLY BASED MODEL FOR PREDICTING THE SUSCEPTIBILITY OF ASPHALT PAVEMENTS TO MOISTURE-INDUCED DAMAGE		5. Report Date September 2010	6. Performing Organization Code
7. Author(s) Rashid K. Abu Al-Rub, Eyad A. Masad, and Michael A. Graham		8. Performing Organization Report No.	
9. Performing Organization Name and Address Texas Transportation Institute Zachry Department of Civil Engineering Texas A&M University College Station, TX 77843-3136		10. Work Unit No. (TRAIS)	11. Contract or Grant No. DTRT07-G-0006
12. Sponsoring Organization Name and Address Southwest Region University Transportation Center Texas Transportation Institute Texas A&M University System College Station, Texas 77843-3135		13. Type of Report and Period Covered	
15. Supplementary Notes Supported by a grant from the U.S. Department of Transportation, University Transportation Centers Program		14. Sponsoring Agency Code	
16. Abstract This study presents a novel moisture-induced continuum damage model for asphalt concrete. Moisture-induced damage is treated realistically as two mechanisms: (1) degradation of the adhesive bond between the asphalt mastic and aggregates and (2) degradation of the cohesive strength of the mastic. The moisture-induced damage model is formulated in a novel way, accounting for the gradual, irreversible degradation of a mix using continuum damage mechanics. Different mechanistic evolution laws are proposed for predicting adhesive and cohesive moisture-induced damage. To the authors' best knowledge, this model is the first continuum model to capture all facets of realistic asphalt mix response. Moreover, a time- and rate-dependent damage constitutive law is proposed to predict crack nucleation and propagation due to different mechanical loading conditions. The moisture-induced and mechanically-induced damage models are integrated into a three-dimensional nonlinear viscoelastic-viscoplastic constitutive model to allow for more realistic prediction of damage evolution in asphalt concrete under various traffic and environmental loading conditions. Numerical integration algorithms are presented for implementing the model in the well-known finite element code Abaqus. Finally, various aspects of the integrated continuum damage mechanics model are investigated and found to match the qualitative behavior of experiments. The current moisture-induced damage model can be used by pavement engineers to predict the time frame over which moisture-induced damage may occur and to rank asphalt mixtures for moisture damage susceptibility.			
17. Key Words Moisture Damage Model; Adhesive Moisture Damage; Cohesive Moisture Damage; Viscoelasticity; Viscoplasticity; Finite Element		18. Distribution Statement No restrictions. This document is available to the public through NTIS: National Technical Information Service Springfield, Virginia 22161 http://www.ntis.gov	
19. Security Classification (of this report) Unclassified	20. Security Classification (of this page) Unclassified	21. No. of Pages 73	22. Price

Physically Based Model for Predicting the Susceptibility of Asphalt Pavements to Moisture-Induced Damage

by

Rashid K. Abu Al-Rub
Zachry Department of Civil Engineering

Eyad A. Masad
Zachry Department of Civil Engineering

and

Michael A. Graham
Zachry Department of Civil Engineering

Performing Agency:
Texas A&M University

Report # SWUTC/10/476660-00012-1

Sponsored by the
Southwest Region University Transportation Center
Texas Transportation Institute
Texas A&M University System
College Station, Texas 77843-3135

September 2010

DISCLAIMER

The contents of this report reflect the views of the authors, who are responsible for the facts and the accuracy of the information presented herein. This document is disseminated under the sponsorship of the Department of Transportation, University Transportation Centers Program in the interest of information exchange. The U.S. Government assumes no liability for the contents or use thereof.

ACKNOWLEDGMENT

The authors recognize that support for this research was provided by a grant from the U.S. Department of Transportation, University Centers Program to the Southwest Region University Transportation Center. Moreover, the authors acknowledge the fruitful discussions they have on moisture-induced damage with Professor Dallas N. Little and Professor Robert L. Lytton from the Zachry Department of Civil Engineering at Texas A&M University.

ABSTRACT

This study presents a continuum-based model for asphalt concrete incorporating nonlinear viscoelasticity, viscoplasticity, mechanically-induced damage, and moisture-induced damage. The Schapery single-integral viscoelastic model describes the nonlinear viscoelastic response. The viscoplastic model of Perzyna models the time-dependent permanent deformations, using a Drucker–Prager yield surface, which is modified to depend on the third deviatoric stress invariant to include more complex dependence on state of stress and to incorporate the different behavior of asphalt concrete under extension and contraction loading conditions. Mechanically-induced damage is modeled using continuum damage mechanics, using the same modified Drucker–Prager law to determine damage onset and growth. A novel moisture damage model is proposed for modeling moisture-induced damage using continuum damage mechanics; adhesive moisture-induced damage to the asphalt mastic–aggregate bond and moisture-induced cohesive damage to the asphalt mastic itself are treated separately. The analytical model is implemented numerically for three-dimensional and plane strain finite element analyses, and a series of simulations is presented to show the performance of the model and its implementation. Sensitivity studies are conducted for all model parameters and results due to various simulations corresponding to laboratory tests are presented. In addition to the continuum model, results are presented for a micromechanical model using the nonlinear-viscoelastic–viscoplastic–damage model for asphalt mastic and a linear elastic model for aggregates. Initial results are encouraging, but basic, and are provided as an example of the model’s robustness and suitability for this task.

EXECUTIVE SUMMARY

Moisture-induced damage has for a long time been recognized by highway agencies and the pavement industry as a serious contributor to premature degradation of asphalt pavements, which leads, in total, to an annual extra vehicle operating cost estimated at more than \$54 billion worldwide. In the last few decades, significant progress has been made in the development of test methods and standards to identify and remediate asphalt mixtures that are prone to moisture damage. However, most of these aimed at trial-and-error comparative measures of moisture damage via visual observations from field data or comparative laboratory tests, which led to very slow advancements in mitigating or alleviating the susceptibility of asphalt pavements to moisture damage. Moreover, these methods do not give any fundamental insight into the causes and evolution of the damage in time within the asphalt mix, nor can they directly be used for mix improvements. Therefore, the main objective of the proposed research effort is to move away from such comparative or empirical measures of moisture damage and develop a fundamental theoretical approach through a mechanistic-based computational continuum damage mechanics framework. This framework will enable realistic predictions and time assessment of the failure pattern occurring in an asphalt pavement under given environmental and traffic loading conditions.

This report presents the development of a continuum-based moisture-induced damage model that can effectively predict the susceptibility of asphalt pavements to premature damage evolution and cracking due to the presence of moisture. The degrading effect due to moisture manifests in two physical phenomena: (1) adhesive moisture damage, ϕ_a^M , which is the degradation of the bond strength between the aggregates and the asphalt mastic due to the existence and diffusion of moisture through the thin films surrounding the aggregate particles and along the aggregate-mastic interfaces; (2) cohesive moisture damage, ϕ_c^M , which is the degradation of the cohesive strength of the asphalt mastic itself. Both (1) and (2) ultimately lead to erosion of the mastic film due to jetting water flow imposed by passing traffic. Therefore, adhesive and cohesive moisture-induced damage mechanisms are modeled using the current continuum damage mechanics framework. Fick's moisture diffusion law is used in order to predict the level of moisture content. Moreover, the moisture-induced damage model is coupled

to constitutive models that can effectively predict the nonlinear viscoelastic, viscoplastic, and time-dependent damage behavior of asphalt concrete.

The Schapery's single-integral nonlinear viscoelastic model is used to predict the nonlinear viscoelastic response of asphalt concrete. The viscoplastic model of Perzyna-type viscoplasticity is adapted in order to predict the time-dependent permanent deformations, where a Drucker–Prager-like yield surface, which is modified to depend on the third deviatoric stress invariant, is used to distinguish between viscoplasticity and damage under extension and contraction loading conditions. Analogous to Perzyna-type viscoplasticity, a time-dependent isotropic damage (viscodamage) evolution law is proposed in this study. The model is capable of describing the damage evolution in asphalt concrete under various loading conditions. The developed moisture-induced continuum damage model, which distinguishes between degradation in the aggregate-mastic interfacial properties and the degradation in the mastic mechanical properties due to the presence of moisture, is coupled to the viscoelastic, viscoplastic, and viscodamage constitutive equations. Finally, a computational algorithm is presented for implementation of the coupled constitutive equations in the well-known commercial finite element code Abaqus via the User MATerial subroutine (UMAT).

Through a systematic parametric study, it is shown that the predictions of the proposed coupled moisture-induced damage model with the viscoelastic, viscoplastic, and viscodamage constitutive equations compare qualitatively well with experimental trends. It is shown that the proposed moisture damage model is advantageous over several exiting moisture-induced damage simulations that do not take into consideration the history of moisture damage evolution. Moreover, these exiting models or simulations all the moisture damage to be completely reversible upon drying, which is not physically sound. It is also demonstrated that the proposed moisture damage modeling framework can be used to conduct micromechanical simulations of the effects of the asphalt concrete constituents on the susceptibility to moisture damage. Therefore, the proposed model can be used ultimately to guide the design of asphalt mixtures with high levels of moisture damage resistance.

Finally, work is currently underway at Texas A&M University for conducting pull-off tests at various moisture conditioning times that can be used for further validation and calibration of the proposed theoretical framework.

TABLE OF CONTENTS

	Page
Abstract.....	vii
Executive Summary.....	ix
List of Figures.....	xiii
List of Tables.....	xv
1 Introduction.....	1
1.1 Literature Review.....	1
1.1.1 Mechanical constitutive modeling of asphalt concrete.....	1
1.1.2 Moisture damage in asphalt concrete.....	3
1.2 Research Approach.....	6
1.3 Research Tasks.....	9
2 Viscoelastic-Viscoplastic Constitutive Model.....	11
2.1 Nonlinear Viscoelasticity.....	12
2.2 Viscoplasticity.....	14
2.2.1 Yield surface.....	15
2.2.2 Viscoplastic potential energy function.....	18
2.2.3 Hardening function.....	18
3 Mechanical-Induced Damage.....	19
3.1 Mechanical Damage Law.....	19
3.1.1 Modified mechanical response.....	19
3.1.2 Damage driving force.....	20
3.1.3 Damage evolution.....	21
3.1.4 Viscodamage law.....	21
3.2 Parametric Study.....	23
4 Moisture-Induced Damage Constutive Model.....	29
4.1 Damage Law.....	29
4.2 Modified Effective Stress.....	31
4.3 Numerical Implementation.....	31
4.3.1 Discrete viscoelastic strain.....	32
4.3.2 Discrete viscoplastic strain.....	33

4.3.3 Computational algorithm for the undamaged configuration	34
4.3.4 Damage implementation	36
4.4 Simulation Results from Moisture-Induced Damage Modeling	38
4.4.1 Moisture damage–mechanical damage coupling	38
4.4.2 Viscoelastic–viscoplastic–mechanical damage–moisture damage model	40
4.4.3 Micromechanical simulations	43
5 Conclusions	49
References	51

LIST OF FIGURES

Figure 1. Moisture-induced damage in pavements results in raveling (left) and potholing (right) (Kringos 2007).	4
Figure 2. Adhesive and cohesive failure (Kringos 2007).	4
Figure 3. Damaged and effective undamaged configurations (Abu Al-Rub and Voyiadjis 2004).	7
Figure 4. Damaged material response without viscoplasticity.	7
Figure 5. The influence of stress path for the modified Drucker-Prager yield surface.	16
Figure 6. Yield surface for plane stress for $d=0.9$ and various values of α	17
Figure 7. Yield surface for plane stress for $\alpha =0.3$ and various values of d	17
Figure 8. The stress-strain relationship for asphalt from a series of uniaxial, compressive constant strain rate tests at various strain rates. The results of two tests at each of the strain rates $\dot{\epsilon}_1 = 0.005$, 0.0005 and 0.00005 are presented (Grenfell 2008).	22
Figure 9. Effect of the damage parameter k^m on the stress-strain response	24
Figure 10. Effect of the damage parameter k^m on the mechanical damage ϕ^m	24
Figure 11. Effect of the threshold damage force Y_{th}^m on the stress-strain response.	26
Figure 12. Effect of the threshold damage force Y_{th}^m on the mechanical damage ϕ^m	26
Figure 13. Effect of the damage force parameter α on the stress-strain response.	27
Figure 14. Effect of the damage force parameter α on the mechanical damage ϕ^m	27
Figure 15. Effect of the damage force parameter d on the stress-strain response.	28
Figure 16. Effect of the damage force parameter d on the mechanical damage ϕ^m	28
Figure 17. Flowchart for numerical implementation of the proposed constitutive model.	37
Figure 18. Stress–strain diagrams due to stress-controlled loads for various moisture exposures.	39
Figure 19. The evolution of damage variable ϕ due to stress-controlled loads with time for various moisture exposures.	39

Figure 20. The evolution of mechanical damage variable ϕ^m due to stress-controlled loads with time for various moisture exposures.	40
Figure 21. Stress–strain and damage evolution plots for constant uniaxial strain rate simulations for several moisture conditioning levels.	41
Figure 22. Stress–strain diagrams for constant uniaxial stress rate simulations for several moisture conditioning levels.	42
Figure 23. Strain vs. time for tensile creep–recovery simulations for several moisture conditioning levels.	42
Figure 24. Von Mises stress distribution due to compressive loading with no moisture exposure.	44
Figure 25. Damage variable distribution due to compressive loading with no moisture exposure.	44
Figure 26. Final moisture distribution.	45
Figure 27. Von Mises stress distribution due to moisture exposure followed by compressive loading.	45
Figure 28. Total damage distribution due to moisture exposure followed by compressive loading. The inset shows adhesive moisture-induced damage.	46
Figure 29. Load–displacement (average stress vs average strain) diagrams for compressive loading with and without moisture exposure.	47

LIST OF TABLES

Table 1. Damage material properties.....	23
Table 2. Viscoelastic and viscoplastic material parameters.	41

1 INTRODUCTION

Roadways are designed to last until rehabilitation or replacement, and it is their degraded performance that dictates the design of pavements. It is, therefore, essential to be able to predict the degradation of an asphalt concrete through the development of a robust computational model that can effectively simulate the performance of an asphalt pavement under mechanical (e.g., traffic) and environmental (e.g., moisture, temperature) loading. Although all materials are heterogeneous, continuum models describe many materials' behavior in a way that allows computation of much more complex physical problems than otherwise feasible. To create a model capable of simulating whole sections of a roadway, this study will use a continuum approach to describe all facets of material behavior. Many past studies have characterized asphalt concrete and its phases using various models (some using continuum models and some using micromechanical approaches), and this section will describe several of these studies and models.

1.1 Literature Review

1.1.1 Mechanical constitutive modeling of asphalt concrete

Experiments show that asphalt concretes deform in a time-dependent manner with recoverable and irrecoverable components and sustain losses of stiffness when subjected to extreme loads (see Perl et al. 1983, Sides et al. 1985, Collop et al. 2003, Grenfell et al. 2008). Cheung and Cebon (1997) and Airey et al. (2002a,b, 2004) studied asphalt binder and determined its response was nonlinear, depending on a combination of temperature and load rate and level. The irrecoverable dilation response of asphalt concrete is overestimated by viscoplasticity with an associated flow rule, so non-associated viscoplasticity must be used to achieve accurate predictions (Masad et al. 2007a). Sousa et al. (1993) developed a nonlinear viscoelastic model for asphalt concrete, which was improved by Sousa et al. (1994) to include plasticity with a von Mises yield surface and isotropic and kinematic hardening. However, this model did not include a pressure-sensitive yield surface or a time-dependent plastic response (viscoplasticity). Ha and Schapery (1999) developed a nonlinear viscoelastic model with damage for particulate composites, but did not model permanent deformations. Seibi et al. (2001) developed a model that used Perzyna's theory of viscoplasticity with a (pressure-sensitive) Drucker–Prager yield surface for the irrecoverable component of deformation, but did not model the time-dependent

character of the recoverable response. Lu and Wright (1998) and Oeser and Moller (2004) developed elasto-viscoplastic constitutive models for asphalt concrete, but did not include a non-associated plastic flow rule. Sadd et al. (2004) used the Schapery nonlinear viscoelasticity model to describe the nonlinear viscoelastic behavior of asphalt concrete with damage in a micromechanical framework, but did not consider irreversible plastic deformations. Kringos, Scarpas, and their collaborators modeled asphalt concrete at a micromechanical level including viscoelasticity and plasticity (for finite strains) and damage, with an emphasis on moisture-induced damage (Kringos 2007, Kringos and Scarpas 2007, Kringos et al. 2008b). Tashman (2003) developed a model for hot mix asphalt that utilized a non-associated viscoplastic flow rule to describe the irreversible component of the deformation. This model accounted for damage, work hardening, and material anisotropy. Levenberg and Uzan (2004) developed a cross-anisotropic viscoelastic-viscoplastic constitutive model for asphalt concrete, but this model did not include viscoplasticity and damage criteria featuring all the dependence on state of stress observed in asphalt concrete, nor did it consider nonlinear viscoelastic response. Dessouky (2005) developed a model that used a modified Drucker–Prager viscoplastic yield surface, which captures the pressure-sensitivity of asphalt concrete, but did not model the nonlinear viscoelastic character for the response. Park et al. (1996) and Park and Schapery (1997) developed a viscoelastic continuum damage model for asphalt concrete, but neglected permanent deformations that are observed in experiments, and their model was limited to uniaxial loading. Chehab et al. (2003) developed a continuum visco-elasto-plastic model for undamaged asphalt concrete, but its scope was also limited to uniaxial characterization. Uzan (2005) developed a damaged-viscoelastic-viscoplastic continuum-based model using the work of Park and Schapery (1997) and Schapery (1999) for asphalt concrete, but did not model three-dimensional response. Masad and co-workers developed a nonlinear-viscoelastic–viscoplastic model for asphalt concrete (Masad et al. 2007b, Huang et al. 2007, Huang 2008, Abu Al-Rub et al. 2009). Schapery’s single-integral theory modeled the nonlinear viscoelastic character of the reversible response and Perzyna’s theory modeled the viscoplastic response using a modified Drucker–Prager yield surface and a non-associated flow rule. The Drucker–Prager yield surface was modified to describe the effect of stress state in a more accurate way than the classical Drucker–Prager yield surface, so that extension loading conditions lead to more viscoplastic flow, apart from hydrostatic pressure state. However, this model did not include damage to the material.

Recently, Darabi et al. (2010) have included into Masad's viscoelastic-viscoplastic framework a viscodamage model that accurately predicts damage evolution in asphalt concrete under different loading conditions.

1.1.2 Moisture damage in asphalt concrete

Moisture damage of asphalt concrete is the degradation of mechanical properties due to the presence of moisture. Moisture damage contributes significantly to the degradation of asphalt pavements; in the U.S., this leads to additional vehicle costs over \$54 billion annually (Copeland 2005). Moisture damage has been studied using a microscale perspective since 1932 and in the field since 1967 (Nicholson 1932, Field and Phang 1967). Much experimental research has sought to determine the degrading effects of moisture, but all purely empirical studies suffer from inability to predict performance, so a description of such work is not included here.

An asphalt mix is a composite material comprised of coarse aggregates, fine aggregates, asphalt binder, and pores, and may be understood as a particulate composite of coarse aggregates and a matrix of *asphalt mastic* (i.e., asphalt binder with fine aggregates) comprised of the other mix constituents. When an asphalt mix is exposed to moisture through water present at its surface (e.g., from rainfall), internally from wet constituents, or through environmental humidity, the moisture disperses through the mix into its air voids and through its solid portion by diffusion and permeation. Once infiltrated by moisture, the mix may be degraded due to several processes: chemical, physical, and mechanical (Kandhal 1994, Kassem 2006, Bhasin 2006, Kringos 2007, Kringos and Scarpas 2007, Caro et al. 2008a).

Figure 1 shows the severe moisture damage resulting in raveling, where aggregates separate from each other individually and potholing, where entire chunks of pavement are removed. Raveling may occur as adhesive failure, where aggregates separate from the mastic, or cohesive failure, where fracture occurs in the mastic between aggregates (Kandhal 1994, Kringos 2007, Caro et al. 2008a). Figure 2 illustrates the difference between adhesive and cohesive failure.

The chemical reactions occurring between moisture and asphalt mix constituents may lead to loss of material that gives the mix its overall cohesion. The overall cohesion is due to a combination of the cohesion of the mastic and maintaining the mastic's adhesion to the aggregates. The cohesion of the aggregates is not included because the matrix cohesion is more essential and because aggregates tend to be very strong and stable compared to the mastic or the aggregate–mastic bond (Little and Jones 2003, Kringos 2007, Caro et al. 2008a). Physical

moisture-induced damage mechanisms are more readily understood and have been studied in some detail (Zollinger 2005, Lytton et al. 2005, Bhasin 2006, Masad et al. 2006c).



Figure 1. Moisture-induced damage in pavements results in raveling (left) and potholing (right) (Kringos 2007).

Physical damage due to moisture occurs when the moisture bonds to the asphalt mix, breaking mastic cohesive or aggregate–mastic adhesive physical bonds. This may lead to debonding of the mastic from aggregates, dispersion of the mastic, possibly lost to flow, and the formation of microcracks in the mix (Kringos 2007, Kringos et al. 2008b, Kringos and Scarpas 2008, Caro et al. 2008a).

Moisture-induced mechanical degradation occurs when the presence of nearly incompressible water in air voids leads to fast-flowing water through the mix upon mechanical loading (e.g., traffic loading), which can cause unfavorable stress distributions and erosion of the mastic (Kandhal 1994, Kringos 2007, Kringos et al. 2008b, Kringos and Scarpas 2008).

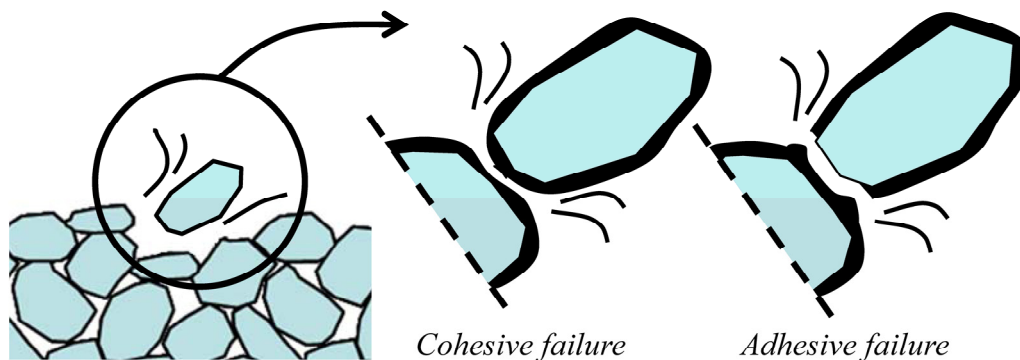


Figure 2. Adhesive and cohesive failure (Kringos 2007).

There are very few studies that have focused on constitutive modeling of moisture-induced damage in hot asphalt mixtures. Recent work studied the fundamental mechanisms of moisture damage, including the role of air voids (Masad et al. 2006b, Kassem 2008), the effects of the physical characteristics of the material and aggregate–binder adhesive bond (Little and Jones 2003, Masad et al. 2006c, Bhasin et al. 2006), and moisture transport in asphalt concrete (Chen et al. 2006, Kassem 2006, Masad et al. 2006a). Caro et al. (2008a,b) modeled asphalt concrete microstructurally, with degradation in the mastic viscoelastic properties and loss of bond at the aggregate–mastic interface using cohesive elements to consider the effect of moisture at the interface and a simple law for damage in the mastic matrix that does not account for irreversibility of moisture-induced damage. Kringos, Scarpas, and their collaborators studied asphalt concrete at the microscale, predicting the infiltration of moisture and the degradation of the material (Kringos and Scarpas 2005, Kringos et al. 2007, Kringos 2007, Kringos and Scarpas 2008, Kringos et al. 2008a,b). Asphalt mastic was modeled using a finite deformation, viscoelastoplastic model. They studied damage at the aggregate–mastic interface and in the body of the mastic due to direct moisture effects and mechanical–moisture coupling effects (pumping). This model neglected irreversibility of moisture damage effects (i.e., moisture-induced damage was recovered upon drying), which is not realistic or physical.

Moisture-induced damage in other materials has also been studied, though generally this research has been microscale rather than continuum modeling. Roy and Xu (2001) and Roy and Benjamin (2004) studied moisture diffusion and damage for polymer matrix composites and graphite/epoxy laminate composites with macroscale application. But this research studied the change in diffusivity of materials due to damage, not the damaging effects of moisture. Chiarelli et al. (2003) developed an elastoplastic damage material model for claystone with properties varying on moisture content, but did not model damage due to moisture independent of mechanical loading. Tang et al. (2005) studied diffusion and moisture-induced damage in woven polymer composites using microscale finite element simulations, but this study focused on the moisture transport due to the special geometry of woven composites, not constitutive modeling of moisture-damaged materials. Roels et al. (2006) proposed a fully coupled mechanical–moisture–damage model and numerical implementation for porous materials, but this model did not include viscoelastic or viscoplastic effects in its mechanical response, and cracks were modeled discretely.

1.2 Research Approach

The proposed constitutive model uses continuum damage mechanics (CDM) framework (Kachanov 1958, 1985), which is a framework for modeling the nucleation, growth, and propagation of numerous microcracks and their evolution into macro-cracks that ultimately lead to failure. CDM is a robust technique that has been used to model degradation in a wide range of materials. CDM can be effectively used in predicting the onset (site and time or where and when) of damage nucleation (cracking potential) and its evolution (crack propagation). In CDM, the effects of the material degradation are explained by explicitly modifying the stiffness of the material sustaining damage. Two configurations are specified: the actual configuration and an equivalent undamaged configuration, which obeys an undamaged material law. The two configurations may be related in various ways, usually based on the assumption that either the strain or the elastic strain energy of the two configurations are equal. The difference between the damaged and undamaged configurations is calculated based on a new parameter, usually called the *damage density* (and this study will use the more general term *damage variable*), which can be calculated due to laws ranging from very simple to laws that incorporate a high degree of realistic physical information for a given material. See Voyiadjis and Kattan (1999), Abu Al-Rub and Voyiadjis (2003) and Lemaitre (2005) for a more complete treatment of continuum damage mechanics.

The simplest example for understanding continuum damage mechanics is the axial bar. Consider a bar with area A_0 and length L , subject to a force F . The stress in the bar is $\sigma = F / A_0$. Now suppose that another bar is identical except that it contains randomly-distributed microcracks and microvoids, so that a proportion ϕ of the cross-sectional area of the bar is removed, so that the area of that bar is $(1-\phi)A_0$. The stress in this bar is $\sigma_\phi = F / [(1-\phi)A_0] = \sigma / (1-\phi)$ (see Figure 3). To an external observer, both bars are the same with an apparent area A_0 , but because of their different areas that are effective in resisting loads, the bar with the microcracks and microvoids will be weaker (lower stiffness and strength). Since the bars are made out of the same material, they have the same material (*effective*) stiffness E_ϕ , but since they have different areas, they respond differently to loads, so a damaged bar with area $(1-\phi)A_0$ has an apparent (*nominal*) stiffness E . Figure 4 shows an example stress-strain diagram for a bar that sustains damage upon increased load. Initially the material is undamaged, so the

nominal and effective stiffness are equal $E = E_\phi$, but upon increased loading the material sustains damage and its stiffness decreases $E < E_\phi$. Upon unloading, the material remains damaged and unloads at the (damaged) nominal stiffness E .

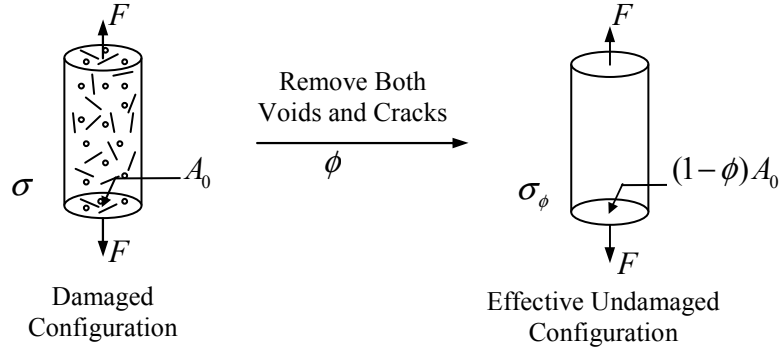


Figure 3. Damaged and effective undamaged configurations (Abu Al-Rub and Voyiadjis 2003).

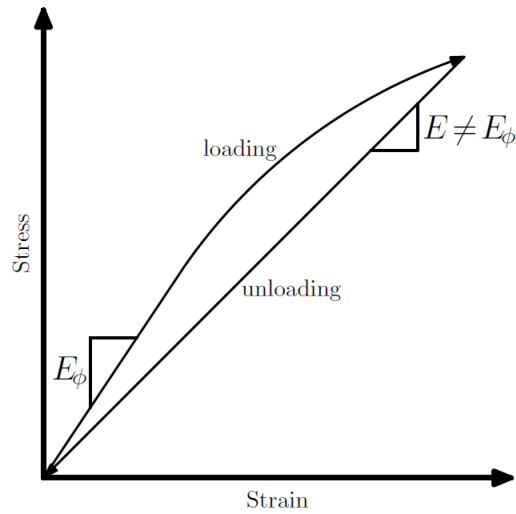


Figure 4. Damaged material response without viscoplasticity.

How is the difference in the mechanical response quantified? The most classical assumption (Kachanov 1958, 1985, Lemaitre 2005) to understand the stiffness change is to hypothesize the strains for the two bars must be equal, so for the strain in the first bar $\dot{\epsilon}$ and the strain in the bar with the reduced area $\dot{\epsilon}_\phi$,

$$\dot{\epsilon} = \dot{\epsilon}_\phi \Rightarrow \frac{\sigma_0}{E} = \frac{\sigma_\phi}{E_\phi} \Rightarrow \frac{F / A_0}{E} = \frac{F / [(1-\phi)A_0]}{E_\phi} \Rightarrow E = (1-\phi)E_\phi \quad (1)$$

The relationships $\dot{\sigma} = \dot{\sigma}_\phi$, $\sigma = (1-\phi)\sigma_\phi$, and $E = (1-\phi)E_\phi$ define the modified constitutive law. This is a common description for the effect of damage, but it will not be used in this research. Suppose instead that the strain energy densities of the two bars are equal. Then:

$$\sigma\dot{\sigma} = \sigma_\phi\dot{\sigma}_\phi \Rightarrow \frac{\sigma^2}{E} = \frac{\sigma_\phi^2}{E_\phi} \Rightarrow \frac{\sigma^2}{E} = \frac{\sigma^2}{(1-\phi)^2 E_\phi} \Rightarrow E = (1-\phi)^2 E_\phi \quad (2)$$

and we also recognize:

$$\sigma_\phi = E_\phi\dot{\sigma}_\phi \Rightarrow \frac{\sigma}{1-\phi} = \frac{E}{(1-\phi)^2}\dot{\sigma}_\phi \Rightarrow \dot{\sigma}_\phi = (1-\phi)\dot{\sigma} \quad (3)$$

The relationships $(1-\phi)\dot{\sigma} = \dot{\sigma}_\phi$, $\sigma = (1-\phi)\sigma_\phi$, and $E = (1-\phi)^2 E_\phi$ define the modified constitutive equations if the strain energy densities for the two bars are equal. For convenience, we wish to perform computations in terms of the nominal strain ε . To do this, we define the effective stress, strain, and stiffness:

$$\begin{aligned} \bar{\sigma} &= \frac{\sigma_\phi}{1-\phi} = \frac{\sigma}{(1-\phi)^2} \\ \bar{\delta} &= \dot{\sigma} \\ \bar{E} &= \frac{E}{(1-\phi)^2} \end{aligned} \quad (4)$$

so that:

$$\bar{\sigma} = \bar{E}\bar{\delta} = \bar{E}\dot{\sigma} \quad (5)$$

This definition is consistent hypothesis that the strain energy densities are equal, but is expressed in terms of the nominal (observable) strain.

CDM can be extended to multiple dimensions. The simplest extension is isotropic damage, in which case Eq. (4) becomes:

$$\begin{aligned} \bar{\sigma}_{ij} &= \frac{1}{(1-\phi)^2} \sigma_{ij} \\ \bar{\delta}_{ij} &= \dot{\sigma}_{ij} \\ \bar{E}_{ijkl} &= \frac{1}{(1-\phi)^2} E_{ijkl} \end{aligned} \quad (6)$$

Throughout this study, tensors are represented using indicial notation. Repeated indices imply summation.

In general, damage need not be isotropic, but can be arbitrarily anisotropic, in which case it may be represented as a second- or fourth-order tensor. This concept is explained by Voyiadjis and Kattan (1999), Abu Al-Rub and Voyiadjis (2003) and Lemaitre (2005). Material isotropy in all facets (viscoelasticity, viscoplasticity, and damage) is assumed in this study for the sake of simplicity. If experiments show that anisotropic damage is necessary to describe the response of asphalt concrete, the proposed model can be modified.

To determine the damage variable φ , material-specific laws that govern the microcracks and microvoids evolution under different loading conditions is needed. Section 3 presents the model for predicting the damage due to mechanical loading, and Section 4 presents the model for predicting the damage due to the presence of moisture.

1.3 Research Tasks

The research objectives will be accomplished by the following tasks:

- The viscoelastic–viscoplastic response will be modeled using Schapery’s single-integral nonlinear viscoelastic model and Perzyna’s viscoplasticity model with a non-associated flow rule, using the same approach as in Huang (2008).
- An analytical model for mechanically-induced damage will be developed, predicting the onset and growth of damage using laws that reflect the physically expected dependence on loading. In particular, damage will be pressure-sensitive, state-of-stress–sensitive, and grow with a physically reasonable law that can be tuned to experimental results.
- An theoretical model for damage due to moisture loading will be developed. The model will meet physical expectations in that the mechanisms of adhesive damage (degradation of the bond between the aggregates and the mastic) and cohesive damage (degradation within the asphalt mastic) will be treated separately, with their initiation and growth described separately, with the option to have the two phenomena behave differently in the model.
- The undamaged material model will be discretized and implemented for finite element simulations in the commercial finite element package Abaqus (2008). Guidelines for this implementation are provided by Huang (2008) and Abu Al-Rub et al. (2009).

- The mechanical and moisture damage laws will likewise be discretized and the undamaged material model implementation will be modified to include damage effects.
- The model and will be tested by running simulations using the numerical implementation in Abaqus (2008) corresponding to realistic loading conditions for mechanical tests.

This report is organized into five sections. This section has introduced and motivated the challenge of modeling the response of asphalt concrete. Section 2 presents the undamaged constitutive model (Huang et al. 2007, Huang 2008, Abu Al-Rub et al. 2009) featuring nonlinear viscoelasticity and viscoplasticity. Section 3 proposes the model for mechanically-induced damage, and Section 4 proposes the model for moisture-induced damage. Section 5 reviews the proposed model and suggests future work for modeling asphalt concrete.

2 VISCOELASTIC-VISCOPLASTIC CONSTITUTIVE MODEL

The proposed damaged constitutive model is based on a model that has been developed for asphalt concrete mixes that describes its nonlinear viscoelastic and viscoplastic response. The viscoelastic model is presented in Masad et al. (2007b) and Huang et al. (2007) and the viscoelastic–viscoplastic model is presented by Huang (2008) and Abu Al-Rub et al. (2009), but the model is described in this section for completeness.

Asphalt concretes are modeled as viscoelastic materials because the recoverable response of asphalt changes with time under constant load and varies for various load rates (Sides et al. 1985, Grenfell et al. 2008) and specifically as nonlinear viscoelastic materials because experiments have shown asphalt binder’s response varies with load level and temperature nonlinearly (Cheung and Cebon 1997, Airey et al. 2002a,b, 2004). It is readily observed that asphalt pavements in service frequently sustain load and recover deformations, so any accurate model for asphalt concrete must include viscoelasticity.

Asphalt concretes are modeled as viscoplastic materials because experiments and observations reveal that asphalt concretes undergo permanent deformation under high or repeated loads, and that the rate at which these permanent deformations accumulate varies with loading rate (Sides et al. 1985, Sousa et al. 1993, 1994; Dessouky 2005, Grenfell et al. 2008). Specifically, a modified Drucker–Prager yield surface and non-associated flow rule are used to conform to empirical observations of asphalt mix response (Dessouky 2005, Masad et al. 2007a). Because excessive permanent deformations may lead to unacceptable pavement performance, any accurate model for asphalt concrete must include viscoplasticity.

The Schapery single-integral nonlinear viscoelastic model (1969) is used for viscoelasticity, and Perzyna’s model (1963, 1966, 1971) is used for viscoplasticity. Asphalt concrete is assumed to be isotropic with constant Poisson’s ratio for the development of this material model. The nonlinear viscoelastic–viscoplastic material model is adapted for numerical use using a recursive-iterative numerical algorithm (as proposed by Haj-Ali and Muliana (2004)) and is implemented in the popular finite element code Abaqus (2008) using a user material subroutine UMAT. Results from finite element simulations in Abaqus are presented.

All values or variables in this section are *effective (undamaged)* values or variables because this section presents the model for the *undamaged material*. The superimposed bars ($\bar{\bullet}$) indicates an effective variable.

2.1 Nonlinear Viscoelasticity

This study employs the Schapery's nonlinear viscoelastic theory to model the recoverable component. Consider the single-integral, nonlinear viscoelastic response (Schapery 1969), which predicts the recoverable time-dependent strain:

$$\dot{\sigma}^{ve}(t) = g_0 \bar{D}_0 \dot{\bar{\sigma}}(t) + \int_0^t g_1 \Delta \bar{D}(\psi(t) - \psi(\tau)) \frac{g_2 \bar{\sigma}(\tau)}{d\tau} d\tau \quad (7)$$

where $\bar{\sigma}(t)$ is the stress at time t , \bar{D}_0 is the instantaneous compliance, $\Delta \bar{D}$ is the transient compliance, $\psi(t)$ is the reduced time, and g_0 , g_1 , and g_2 are nonlinear parameters explained below. Time $t = 0$ is some time before loading. A nonlinear viscoelastic model was chosen due to the observations of Cheung and Cebon (1997) and Airey et al. (2002a,b, 2004). *Throughout this report positive values of stress and strain represent compression, as is the typical convention for pressure-sensitive materials.*

The reduced time:

$$\psi(t) = \int_0^t \frac{d\xi}{a_T(\xi) a_s(\xi)} \quad (8)$$

adjusts the time the transient compliance is evaluated using the temperature shift factor a_T and the stress or strain shift factor a_s , and other shift factors may be postulated if necessary. The reduced time adjusts the predictions of Eq. (7) due to the effects of temperature and stress or strain (or any other inputs that are experimentally observed to modify response in a time-shifting manner) by conforming to the response predicted for a different loading rate.

The nonlinear parameter g_0 relates to the instantaneous compliance, the nonlinear parameter g_1 relates to the transient compliance, and the nonlinear parameter g_2 relates to the effect of the loading rate on response. The nonlinear parameters g_0 , g_1 , and g_2 may be functions of stress, strain, loading rate, temperature, moisture, etc., and may be empirically determined based on observed nonlinearity. g_0, g_1 , and g_2 are positive and for small values of stress should be close to unity; if $g_0 = g_1 = g_2 = 1$, Eq. (7) reduces to the Boltzmann integral in linear viscoelasticity (Haj-Ali and Muliana 2004).

To use this formulation to solve three-dimensional problems, we recall from linear elasticity that the strain $\dot{\epsilon}_{ij}^{ve}$ for an isotropic material may be decomposed into deviatoric strain e_{ij}^{ve} and volumetric strain $\dot{\epsilon}_{kk}^{ve}$:

$$\dot{\epsilon}_{ij}^{ve} = \underbrace{\frac{1}{2}\bar{J}\bar{S}_{ij}}_{e_{ij}^{ve}} + \underbrace{\frac{1}{3}\bar{B}\bar{\sigma}_{kk}}_{\dot{\epsilon}_{kk}^{ve}} \delta_{ij} \quad (9)$$

where \bar{J} is the undamaged shear compliance, \bar{B} is the undamaged bulk compliance, \bar{S}_{ij} is the deviatoric stress:

$$\bar{S}_{ij} = \bar{\sigma}_{ij} - \frac{\bar{\sigma}_{kk}}{3} \delta_{ij},$$

$\bar{\sigma}_{kk}$ is the volumetric stress, and δ_{ij} is the Kronecker delta:

$$\delta_{ij} = \begin{cases} 1 & \text{if } i = j \\ 0 & \text{if } i \neq j \end{cases}$$

Using the Schapery single-integral model, Eq. (7), the viscoelastic deviatoric and volumetric strains are expressed as:

$$\begin{aligned} e_{ij}^{ve}(t) &= \frac{1}{2}g_0(t)\bar{J}_0\bar{S}_{ij}(t) + \frac{1}{2}g_1(t)\int_0^t \Delta\bar{J}(\psi(t)-\psi(\tau)) \frac{d(g_2(\tau)\bar{S}_{ij}(\tau))}{d\tau} d\tau, \\ \dot{\epsilon}_{kk}^{ve}(t) &= \frac{1}{3}g_0(t)\bar{B}_0\bar{\sigma}_{kk}(t) + \frac{1}{3}g_1(t)\int_0^t \Delta\bar{B}(\psi(t)-\psi(\tau)) \frac{d(g_2(\tau)\bar{\sigma}_{kk}(\tau))}{d\tau} d\tau, \end{aligned} \quad (10)$$

where the meanings of the new terms should be obvious: \bar{J}_0 is the instantaneous shear compliance, $\Delta\bar{J}(t)$ is the transient shear compliance, \bar{B}_0 is the instantaneous bulk compliance, and $\Delta\bar{B}(t)$ is the transient bulk compliance.

Experimental measurements have shown that the Poisson's ratio ν for asphalt concrete mixes varies some with time, temperature, or loading rate, but the simplification that ν is time-independent is adopted for this material model because the effect of this small variation is minor compared to other effects (ASTM 1995, Di Benedetto et al. 2007). This leads to the modulus interrelations:

$$\begin{aligned} \bar{J}_0 &= 2(1-\nu)\bar{D}_0 & \bar{B}_0 &= 3(1-2\nu)\bar{D}_0 \\ \Delta\bar{J}(t) &= 2(1-\nu)\Delta\bar{D}(t) & \Delta\bar{B}(t) &= 3(1-2\nu)\Delta\bar{D}(t) \end{aligned} \quad (11)$$

Note only one independent function of time is part of the analysis.

The transient compliance $\Delta D(t)$ is represented by the Prony series:

$$\Delta \bar{D}(t) = \sum_{n=1}^{N_p} \bar{D}_n (1 - e^{-\lambda_n t}) \quad (12)$$

where for the N_p modes, D_n is the coefficient of the Prony series in mode n and λ_n is the retardation time in mode n .

Substituting the transient compliance from Eq. (12) into Eq. (10) yields:

$$\begin{aligned} e_{ij}^{ve}(t) &= \frac{g_0(t) \bar{J}_0 \bar{S}_{ij}(t)}{2} + \frac{g_1(t)}{2} \int_0^t \sum_{n=1}^{N_p} \bar{J}_n \left(1 - e^{-\lambda_n (\psi(t) - \psi(\tau))} \right) \frac{d(g_2(\tau) \bar{S}_{ij}(\tau))}{d\tau} d\tau \\ \dot{\epsilon}_{kk}^{ve}(t) &= \frac{g_0(t) \bar{B}_0 \bar{\sigma}_{kk}(t)}{3} + \frac{g_1(t)}{3} \int_0^t \sum_{n=1}^{N_p} \bar{B}_n \left(1 - e^{-\lambda_n (\psi(t) - \psi(\tau))} \right) \frac{d(g_2(\tau) \bar{\sigma}_{kk}(\tau))}{d\tau} d\tau \end{aligned} \quad (13)$$

which serve as the governing equations for the viscoelastic strain.

2.2 Viscoplasticity

In addition to the recoverable viscoelastic strain, experiments indicate some strain in asphalt concrete mixes is irrecoverable with time-dependent response, so we divide the strain $\dot{\epsilon}_{ij}$ into recoverable viscoelastic strain $\dot{\epsilon}_{ij}^{ve}$ and irrecoverable viscoplastic strain $\dot{\epsilon}_{ij}^{vp}$ (assuming small strains) or the:

$$\dot{\epsilon}_{ij} = \dot{\epsilon}_{ij}^{ve} + \dot{\epsilon}_{ij}^{vp} \quad (14)$$

Taking the time derivative of this expression, the strain rate is

$$\ddot{\epsilon}_{ij} = \ddot{\epsilon}_{ij}^{ve} + \ddot{\epsilon}_{ij}^{vp} \quad (15)$$

for the viscoelastic strain rate $\dot{\epsilon}_{ij}^{ve}$ and the viscoplastic strain rate $\dot{\epsilon}_{ij}^{vp}$.

This study uses Perzyna's model (1963, 1966, 1971) to calculate the viscoplastic strain rate:

$$\dot{\epsilon}_{ij}^{vp} = \begin{cases} \Gamma \left(\frac{f}{\sigma_y^0} \right)^N \frac{\partial g}{\partial \bar{\sigma}_{ij}}, & \text{if } f \geq 0 \\ 0, & \text{if } f < 0 \end{cases} \quad (16)$$

where f is the yield surface, g is the viscoplastic potential energy function, Γ is a viscosity parameter, σ_y^0 is a parameter which normalizes stress values, and N is a parameter describing rate-dependence. The rate of viscoplastic strain is controlled by the scalar $\Gamma (f / \sigma_y^0)^N$ when the

overstress function (f / σ_y^0) is positive, and the direction is controlled by the tensor $\partial g / \partial \bar{\sigma}_{ij}$. If the yield surface function does not coincide with the potential energy function ($f \neq g$), Eq. (16) is a non-associated viscoplastic flow rule.

2.2.1 Yield surface

The yield surface determines whether a stress state results in viscoplastic strain. This study uses a modified Drucker–Prager yield surface:

$$f = \bar{\tau} - \alpha \bar{I}_1 - \kappa (\delta_e^{vp}) \quad (17)$$

where $\bar{\tau}$ and \bar{I}_1 are stress invariants, α is a pressure-sensitivity parameter related to the angle of friction in the mix, and κ is the viscoplastic hardening function, which depends on the equivalent viscoplastic strain δ_e^{vp} .

Consider $\tau - \alpha I_1$. \bar{I}_1 is the first stress invariant:

$$\bar{I}_1 = \frac{1}{3} \bar{\sigma}_{ii} \quad (18)$$

which is the effective hydrostatic pressure. $\bar{\tau}$ is the effective deviatoric shear stress modified for the stress state:

$$\bar{\tau} = \frac{\sqrt{\bar{J}_2}}{2} \left(1 + \frac{1}{d} + \left(1 - \frac{1}{d} \right) \frac{\bar{J}_3}{\sqrt{\bar{J}_2^3}} \right) \quad (19)$$

where \bar{J}_2 and \bar{J}_3 are the second and third effective deviatoric stress invariants:

$$\begin{aligned} \bar{J}_2 &= \frac{3}{2} \bar{S}_{ij} \bar{S}_{ij} \\ \bar{J}_3 &= \frac{9}{2} \bar{S}_{ij} \bar{S}_{jk} \bar{S}_{ki} \end{aligned} \quad (20)$$

and d is a material parameter describing sensitivity to extension, regardless of hydrostatic state.

Figure 5 shows the influence of stress path on the response using the modified Drucker-Prager yield surface, plotted in the $I_1 - \sqrt{J_2}$ plane. Note that damage is not considered in drawing Figure 5. For a classical Drucker-Prager yield surface, $\alpha = \alpha'$ and $\kappa = \kappa'$, but the parameter d causes them to be different for the modified Drucker-Prager surface.

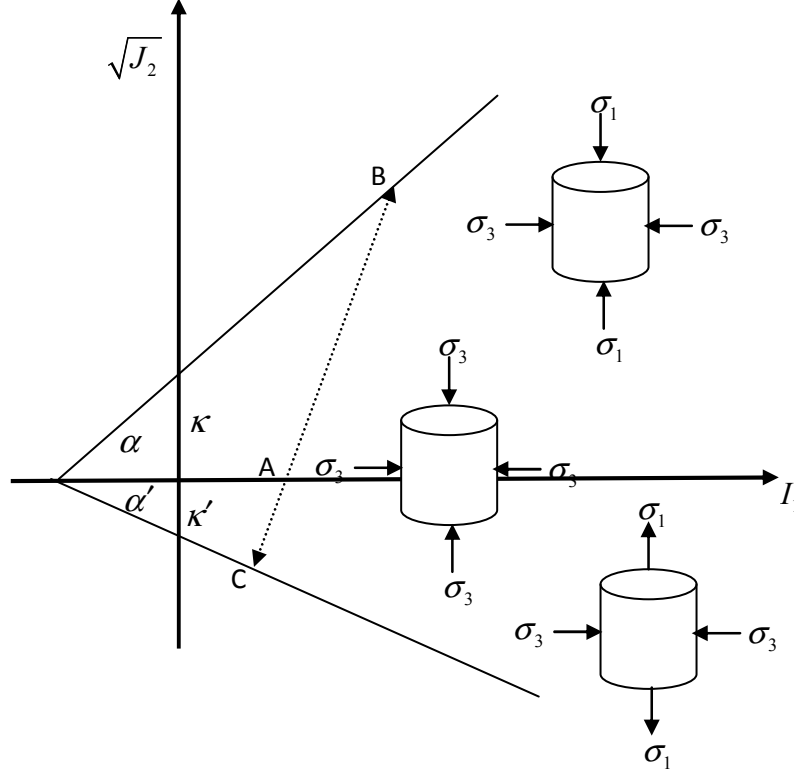


Figure 5. The influence of stress path for the modified Drucker-Prager yield surface.

To better understand the yield surface, consider a body loaded in plane stress with principal stresses $\bar{\sigma}_1$ and $\bar{\sigma}_2$ (all other stress components are zero). Then:

$$\begin{aligned}
 \bar{I}_1 &= \frac{1}{3}(\bar{\sigma}_1 + \bar{\sigma}_2) \\
 \bar{J}_2 &= \bar{\sigma}_1^2 - \bar{\sigma}_1\bar{\sigma}_2 + \bar{\sigma}_2^2 \\
 \bar{J}_3 &= \frac{1}{2}(2\bar{\sigma}_1 - \bar{\sigma}_2)(\bar{\sigma}_1 + \bar{\sigma}_2)(\bar{\sigma}_1 - 2\bar{\sigma}_2)
 \end{aligned} \tag{21}$$

so the yield surface in Eq. (17) becomes:

$$\begin{aligned}
 &\frac{\bar{\sigma}_1^2 - \bar{\sigma}_1\bar{\sigma}_2 + \bar{\sigma}_2^2}{2} \left(1 + \frac{1}{d} + \left(1 - \frac{1}{d} \right) \frac{(2\bar{\sigma}_1 - \bar{\sigma}_2)(\bar{\sigma}_1 + \bar{\sigma}_2)(\bar{\sigma}_1 - 2\bar{\sigma}_2)}{2(\bar{\sigma}_1^2 - \bar{\sigma}_1\bar{\sigma}_2 + \bar{\sigma}_2^2)^{3/2}} \right) \\
 & - \frac{\alpha}{3}(\bar{\sigma}_1 + \bar{\sigma}_2) - \kappa(\delta_e^{vp}) = 0
 \end{aligned} \tag{22}$$

We may now plot the yield surface in the $\bar{\sigma}_1 - \bar{\sigma}_2$ plane.

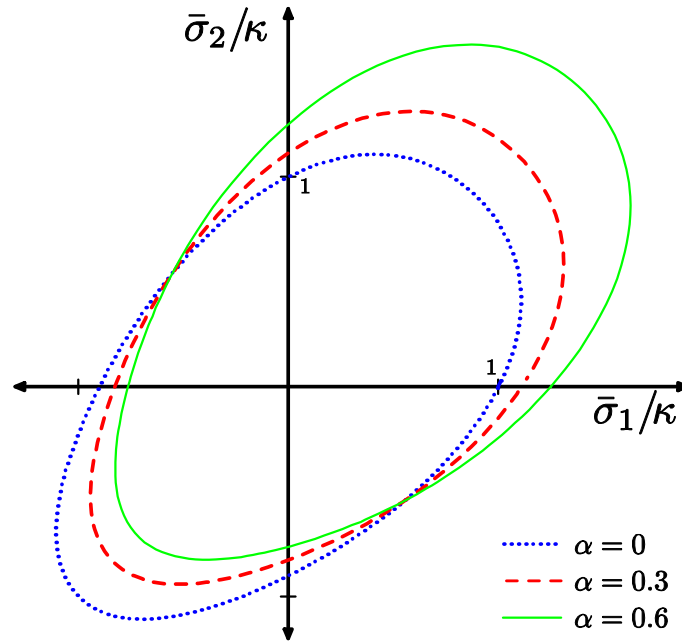


Figure 6. Yield surface for plane stress for $d=0.9$ and various values of α .

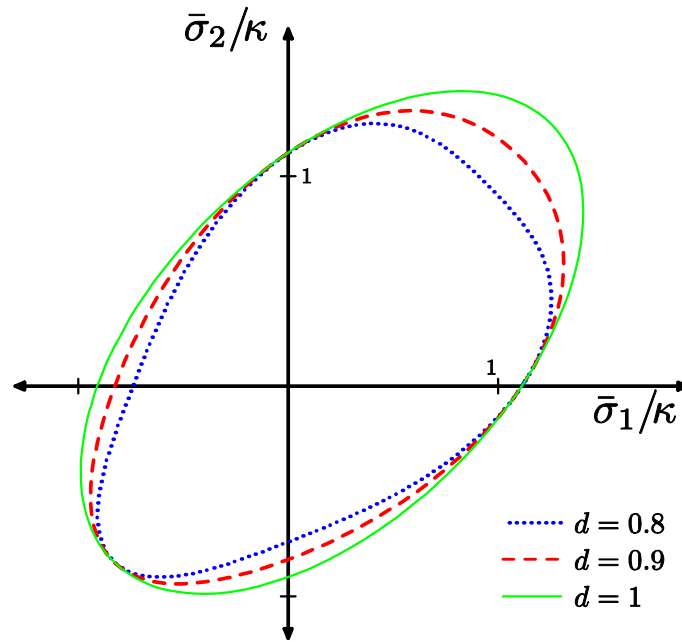


Figure 7. Yield surface for plane stress for $\alpha=0.3$ and various values of d .

Figure 6 and Figure 7 show the yield surface for plane stress with principal stresses $\bar{\sigma}_1$ and $\bar{\sigma}_2$ normalized by the isotropic hardening function $\kappa(\delta_e^{vp})$.

2.2.2 Viscoplastic potential energy function

In asphalt concrete mixes, the direction of the viscoplastic strain growth is not normal to the yield surface, which is called non-associated flow, and an associated flow rule would overestimate the dilation compared to experimental measurements (Masad et al. 2007a). This study defines the viscoplastic potential energy function:

$$g = \bar{\tau} - \beta \bar{I}_1 \quad (23)$$

which is similar to the yield surface, except the material parameter β governs the pressure sensitivity of the surface.

The derivative in Eq. (16) is calculated to be $\partial g / \partial \bar{\sigma}_{ij}$:

$$\frac{\partial g}{\partial \bar{\sigma}_{ij}} = \frac{1}{2} \left[\left(1 + \frac{1}{d} \right) \frac{3\bar{S}_{ij}}{2\sqrt{\bar{J}_2}} + \left(1 - \frac{1}{d} \right) \frac{3 \left(\frac{9}{2} \bar{S}_{ik} \bar{S}_{kj} - \bar{J}_2 \delta_{ij} \right) \bar{J}_2 - 3\bar{S}_{ij} \bar{J}_3}{\bar{J}_2^2} - \frac{2\beta}{3} \delta_{ij} \right] \quad (24)$$

2.2.3 Hardening function

The evolution of the yield surface, Eq. (17), depends on the isotropic hardening function κ , for which the isotropic hardening rule:

$$\kappa(\dot{\epsilon}_e^{vp}) = \kappa_0 + \kappa_1 \left(1 - \exp(-\kappa_2 \dot{\epsilon}_e^{vp}) \right) \quad (25)$$

is used (Lemaitre and Chaboche 1990), where κ_0 defines the initial yield stress, $\kappa_0 + \kappa_1$ describes the saturated stress for the fully-hardened material, κ_2 describes the transition rate between κ_0 and $\kappa_0 + \kappa_1$, and:

$$\dot{\epsilon}_e^{vp} = \int_0^t \dot{\epsilon}_e^{vp} dt \quad (26)$$

is the equivalent viscoplastic strain, where time $t=0$ is some time before viscoplastic deformation. We use the equivalent plastic strain rate as defined in Huang (2008) based on viscoplastic work in uniaxial compression, such that:

$$\dot{\epsilon}_e^{vp} = \sqrt{\frac{\left(1 - \frac{\beta}{3} \right)^2 \dot{\sigma}_{ij}^{vp} \dot{\sigma}_{ij}^{vp}}{\left(1 - \frac{\beta}{3} \right)^2 + 2 \left(\frac{1}{2} + \frac{\beta}{3} \right)^2}} \quad (27)$$

3 MECHANICAL-INDUCED DAMAGE

One major cause of degradation in asphalt pavements is mechanical loading of the pavements, especially due to trucks driving over asphalt roadways, so a thorough constitutive model describing the degradation of asphalt pavements must include the effects of mechanical loads. The proposed model uses CDM to model the degradation of an asphalt concrete body subject to mechanical loads. Modeling asphalt concrete (and composite materials in general) requires some generalization of CDM because it is unreasonable to assume microcracks and microvoids are distributed completely randomly, since an asphalt mix is very heterogeneous at the scale of microcracks. Further, the phases of asphalt concrete mixes vary greatly in their contributions to the strength and stiffness of a mix, so it is not reasonable to equate the damage variable to the proportion of the material occupied by microcracks and microvoids. However, asphalt concretes exhibit damage behavior like that predicted by CDM: as loading becomes severe, the material softens and when it is unloaded, its stiffness is reduced compared to the recovery stiffness after less severe loading. Therefore, CDM is used with the damage variable ϕ^m , which does not indicate any specific volumetric distribution of microcracks and voids, but instead arises directly from the energy dissipated through fracture causing loss of strength and stiffness of the material, and is the proper quantity to indicate the amount of stiffness that is lost.

3.1 Mechanical Damage Law

3.1.1 Modified mechanical response

The mechanically-induced damage relates the predicted response to that of the undamaged material by:

$$\bar{\sigma}_{ij}(t) = \frac{\sigma_{ij}(t)}{(1 - \phi^m(t))^2} \quad (28)$$

where σ_{ij} is the *nominal stress* for the body and $\bar{\sigma}_{ij}$ is the *effective stress*, which is the stress level experienced by the material still effective at resisting loads, which is calculated using the undamaged viscoelastic–viscoplastic model presented in Section 2. In fact, one can refer to σ_{ij} is the *apparent stress* that is measured experimentally whereas $\bar{\sigma}_{ij}$ is the *true stress* that will cause

further viscoelasticity, viscoplasticity, and damage. This is why the constitutive equations presented in the previous sections are presented in terms of $\bar{\sigma}_{ij}$. The Abaqus UMAT subroutine can then be modified according to this relation: the stress used for the finite element mesh is the nominal stress, but the undamaged material model is used to calculate the effective stress $\bar{\sigma}_{ij}$. The two stresses relate by ϕ^m , which is calculated as described in this section.

3.1.2 Damage driving force

The driving force for mechanical damage postulated to be:

$$Y^m = \bar{\tau} - \alpha \bar{I}_1, \quad \bar{\tau} = \frac{\sqrt{3\bar{J}_2}}{2} \left(1 + \frac{1}{d^d} + \left(1 - \frac{1}{d^d} \right) \frac{\bar{J}_3}{\sqrt{3\bar{J}_2^3}} \right) \quad (29)$$

where \bar{I}_1 , \bar{J}_2 , and \bar{J}_3 are stress invariants (calculated from the *effective stress* $\bar{\sigma}_{ij}$) and α and d^d are material parameters that are already defined for the viscoplastic yield surface in Section 3. This form resembles the viscoplastic yield surface and is appropriate because its properties reflect the physical behavior of asphalt concrete. d^d is the parameter that distinguishes between damage under extension (e.g., tension) and damage under contraction (e.g., compression) loading conditions, which can be different than d for viscoplasticity, Eq. (19).

The mechanical damage is based on the state of stress, so the driving force increases more severely depending on the state of stress. The mechanical damage is *pressure sensitive*, so that for tensile states of stress, the driving force is greater than for an analogous compressive state of stress, which in this model is due to the term $\alpha \bar{I}_1$, such that (for $\alpha > 0$) compressive pressures $\bar{I}_1 > 0$, the damage force is less than $\bar{\tau}$ and for tensile pressures $\bar{I}_1 < 0$, the damage force is greater than $\bar{\tau}$. The mechanical damage is sensitive to extension, so that extensions *even under hydrostatic compression*, the damage force is greater for extensions in a compressive case than further compressions; this effect is due to the form of $\bar{\tau}$ and is controlled by the constant d^d . If $d^d = 1$, this effect vanishes and $\bar{\tau}$ is exactly the von Mises stress; as d^d decreases, this effect is amplified. Because the proposed damage model has a damage surface that is analogous to the viscoplastic yield surface, one can refer to Figure 6 and Figure 7 for the effect of the damage material parameters.

3.1.3 Damage evolution

The evolution of damage is treated similarly to viscoplasticity. To determine whether damage occurs and how it evolves through time, a damage surface G is defined to be:

$$G = Y^m - Y_{th}^m \leq 0, \quad (30)$$

where Y^m is the damage force (defined in the previous section) and Y_{th}^m is the *threshold damage force*, which is the damage force for which damage starts to occur. Should the damage surface G reach 0, damage occurs, leading to the condition:

$$G = Y^m - Y_{th}^m - \kappa_\phi(\phi^m) = 0 \quad (31)$$

where $\kappa_\phi(\phi^m)$ is the *isotropic damage function*, which governs the evolution of the damage. For this study we choose:

$$\kappa_\phi(\phi^m) = \frac{Y_{th}^m}{k^m} \ln(1 - \phi^m) \quad (32)$$

where k^m is the mechanical damage growth parameter, which governs the evolution rate of damage. To gain greater intuition and for numerical implementation, we substitute Eqs. (31) and (32), and rearrange to yield:

$$\phi^m = 1 - \exp \left[-k^m \left(\frac{Y^m}{Y_{th}^m} - 1 \right) \right] \quad (33)$$

This model is chosen because it matches the physical expectations that (a) when damage first occurs, its value is $\phi^m = 0$, (b) damage accumulates more and more as loading becomes more severe, and (c) the damage variable will not exceed unity ($\phi^m < 1$), and because exponential damage growth has frequently been observed in experiments for other materials (Cicekli et al. 2007, Abu Al-Rub and Voyiadjis 2009).

3.1.4 Viscodamage law

However, experiments have indicated that the damage accumulation in asphalt mixes is dependent on the load history (Grenfell et al. 2008). Consider the experimental results of uniaxial, compressive constant strain rate tests shown in Figure 8. At faster strain rates, the asphalt concrete is more resilient in resisting loads. It exhibits stiffer initial (viscoelastic) response, then in the viscoplastic-damaged regime, the same qualitative behavior occurs at

higher stresses and slightly higher strains. The damage model presented in Eq. (33) is rate- and time-independent and is not suitable for predicting damage evolution in asphalt mixtures. Therefore, the model needs to be modified in order to include viscous effects (i.e., rate- and time-dependent behavior). The viscodamage model that has been formulated by Voyiadjis et al. (2004) based on laws of thermodynamics is employed here such that Eq. (31) can be written as

$$\dot{\phi}^m = \Gamma^{vd} \left(\frac{G}{Y_{th}^m} \right)^\zeta \quad (34)$$

where Γ^{vd} is the damage viscosity parameter that controls how fast damage occurs and has the units of 1/second such that $1/\Gamma^{vd}$ designates the damage relaxation time similar to relaxation times in viscoelasticity and viscoplasticity constitutive equations. The parameter ζ controls the damage rate-sensitivity, and $G \geq 0$ is given in Eq. (31). In fact, one can notice that this damage law is analogous to the Perzyna viscoplastic flow rule in Eq. (16).

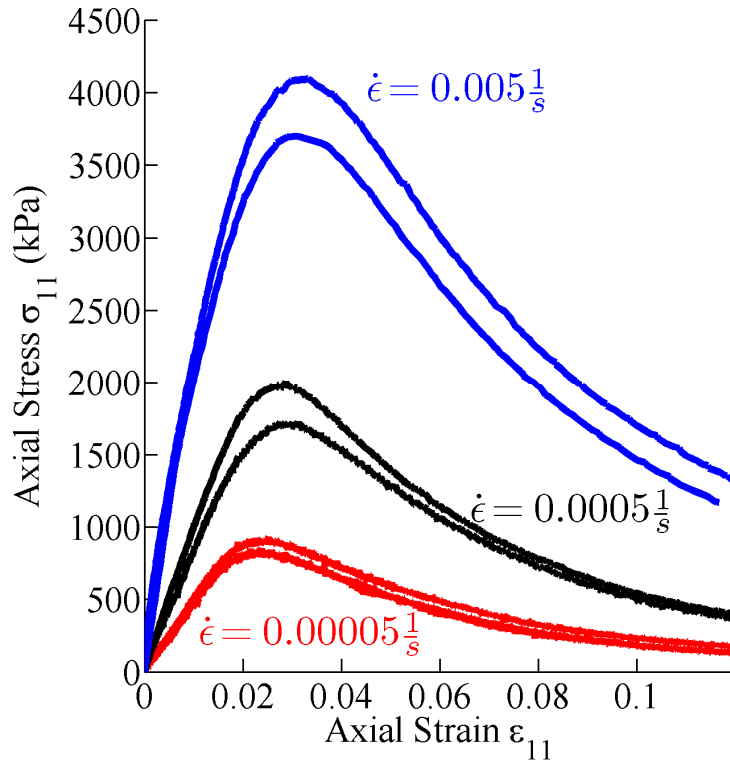


Figure 8. The stress-strain relationship for asphalt from a series of uniaxial, compressive constant strain rate tests at various strain rates. The results of two tests at each of the strain rates $\dot{\epsilon}_1 = 0.005$, 0.0005 and 0.00005 are presented (Grenfell et al. 2008).

3.2 Parametric Study

Two material parameters, Y_{th}^m and k^m , are introduced for mechanical damage, and two more, α and d^d (in this study assumed $d^d = d$) affect the mechanical damage and are already defined for viscoplasticity. To understand them, a parametric sensitivity study examines the various parameters' effects on the response and their experimental determination is discussed.

This section presents the results of a parametric study for all of the damage material parameters. The results are from a series of simulations in Abaqus (2008). The results are reported at one integration point subjected to uniaxial strain at a constant strain rate $\dot{\delta} = 0.0015s^{-1}$ for 60 seconds. In all cases uniaxial compression was simulated and in some cases it was deemed important to present results from simulations of uniaxial tension; when tensile simulation results are reported, they are plotted on the same axes as compression results with dashed lines. All material parameters are held constant at the values from Table 1 except the parameter being studied, which is varied with one larger and one smaller value.

Table 1. Damage material properties.

Property (Unit)	Value
Y_{th}^m (kPa)	2000
k^m	0.08
α	0.3
d	0.9
Γ^{vd} (1/second)	10^{-5}
ζ	1

Figure 9 shows how the stress-strain response changes due to varying the mechanical damage parameter k^m , and Figure 10 shows the evolution of the mechanical damage variable ϕ^m through the simulations of varying k^m . After damage begins to accumulate when the damage force Y^m reaches the threshold damage force Y_{th}^m , the mechanical damage parameter controls the severity of damage, where larger values of k^m indicate more damage (larger values of ϕ^m) and hence a less stiff material.

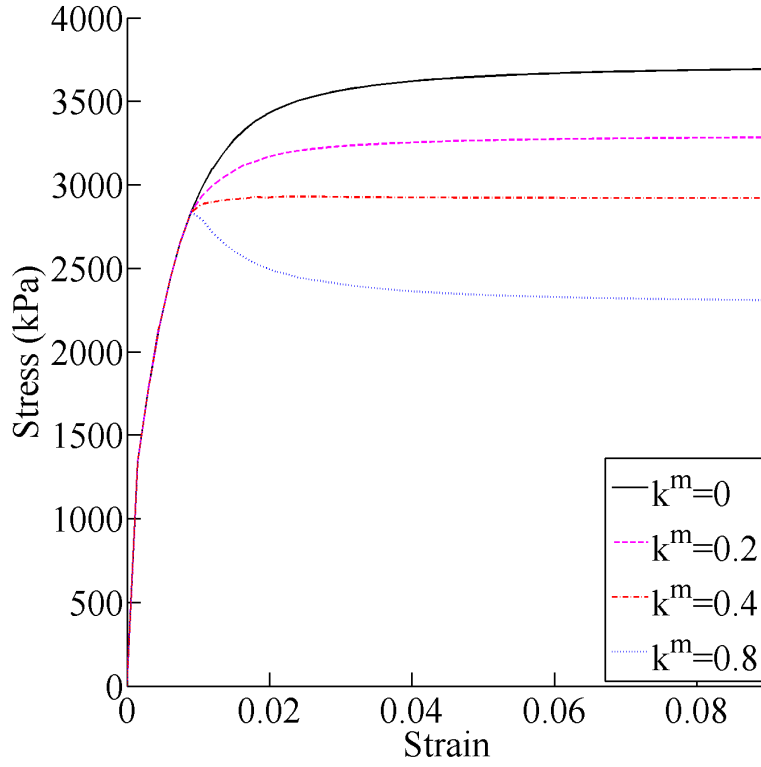


Figure 9. Effect of the damage parameter k^m on the stress-strain response.

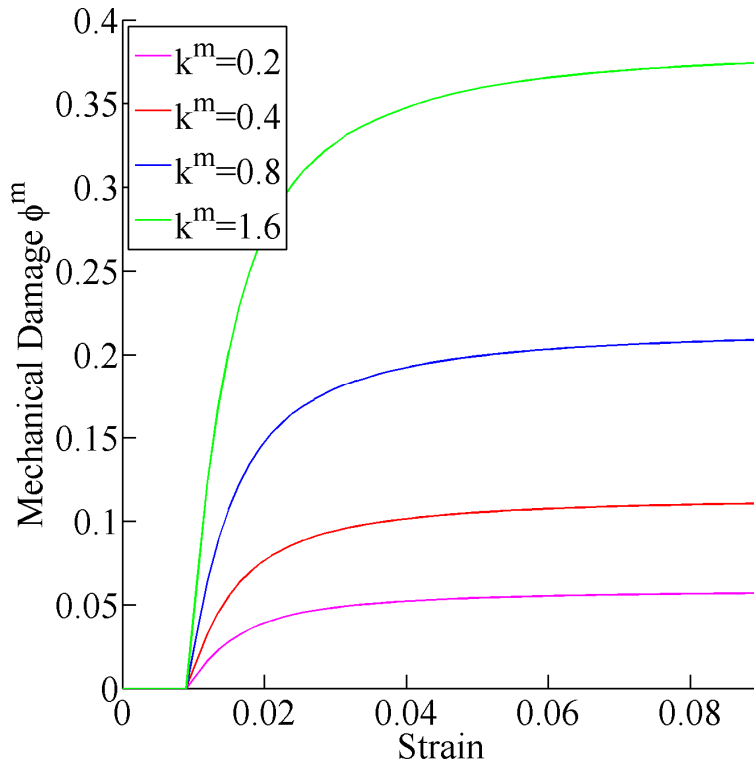


Figure 10. Effect of the damage parameter k^m on the mechanical damage ϕ^m .

Figure 11 shows how the stress-strain response changes due to varying the threshold mechanical damage force Y_{th}^m , and Figure 12 shows the evolution of the mechanical damage variable ϕ^m through the simulations varying Y_{th}^m . All else held equal, large values of Y_{th}^m cause damage to begin later, and to be less severe.

Remember when examining Figure 13–Figure 16 that varying α and d also affects the viscoplastic response of the material. Figure 13 shows how the stress-strain response changes due to varying the parameter α , and Figure 14 shows the evolution of the mechanical damage variable ϕ^m through the simulations varying α . As α decreases, the compressive and tensile stress-strain behaviors become more similar, as α introduces pressure sensitivity to the model. Larger values of α result in less mechanical damage in compression and more mechanical damage in tension.

The results for the effect of d are most clearly seen in a stress-controlled regime, so Figure 15 and Figure 16 present the results of constant stress rate tests with the stress rates $\dot{\sigma} = 58.3\text{kPa/s}$ for compression and $\dot{\sigma} = 28.3\text{kPa/s}$ for tension. Figure 15 shows how the stress-strain response changes due to varying the parameter d , and Figure 16 shows the evolution of the mechanical damage variable ϕ^m through the constant stress rate simulations varying d .

As emphasized earlier, time-, rate-, and temperature-independent evolution equations for the damage variable, ϕ , are not proper to predict the damage nucleation and growth in asphaltic materials. Recently, Darabi et al. (2010) proposed the following thermo-viscodamage evolution law:

$$\dot{\phi}^m = \Gamma_0^{vd} \left[\frac{Y^m}{Y_0} \right]^q (1 - \phi)^2 \exp(k \varepsilon_{eff}) \exp\left(\zeta \frac{T - T_0}{T_0}\right) \quad (35)$$

where Γ_0^{vd} is the reference damage viscosity, q is the stress-dependency parameter, Y_0 is the reference damage force, k is a material parameter, and $\varepsilon_{eff} = \sqrt{\varepsilon_{ij} \varepsilon_{ij}}$ is the effective or equivalent total strain, ζ describes how much the damage rate can be affected when temperature changes T , and T_0 is the reference temperature. This damage evolution law and its coupling to moisture damage constitutive equations are currently under investigation at Texas A&M University to see how they affect the moisture-induced damage in asphalt concrete.

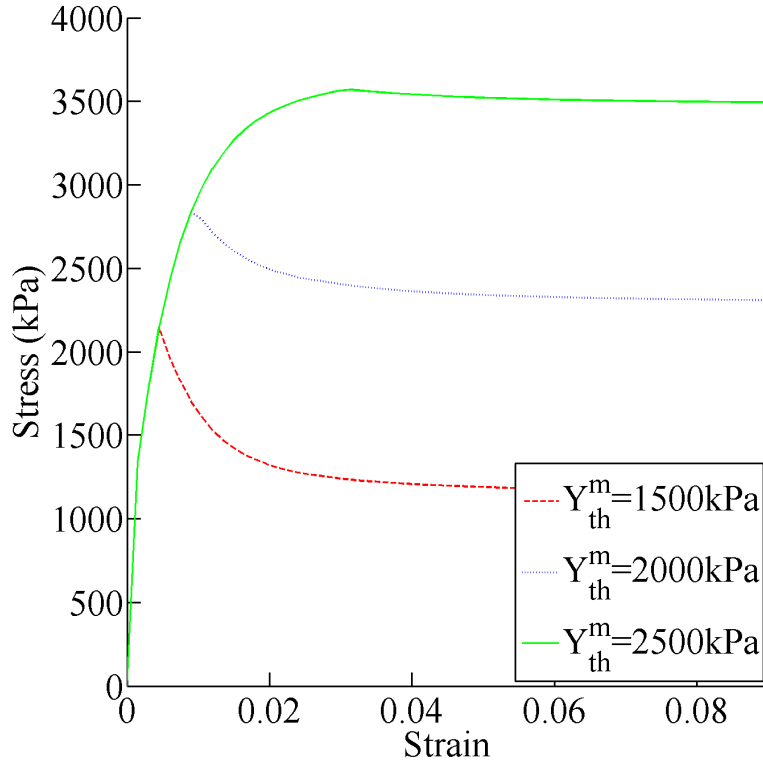


Figure 11. Effect of the threshold damage force Y_{th}^m on the stress-strain response.

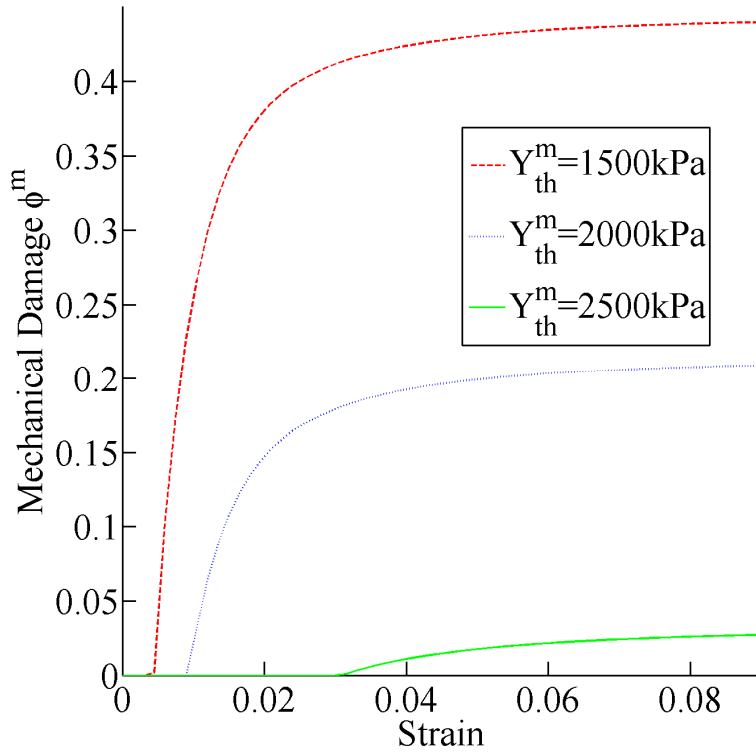


Figure 12. Effect of the threshold damage force Y_{th}^m on the mechanical damage ϕ^m .

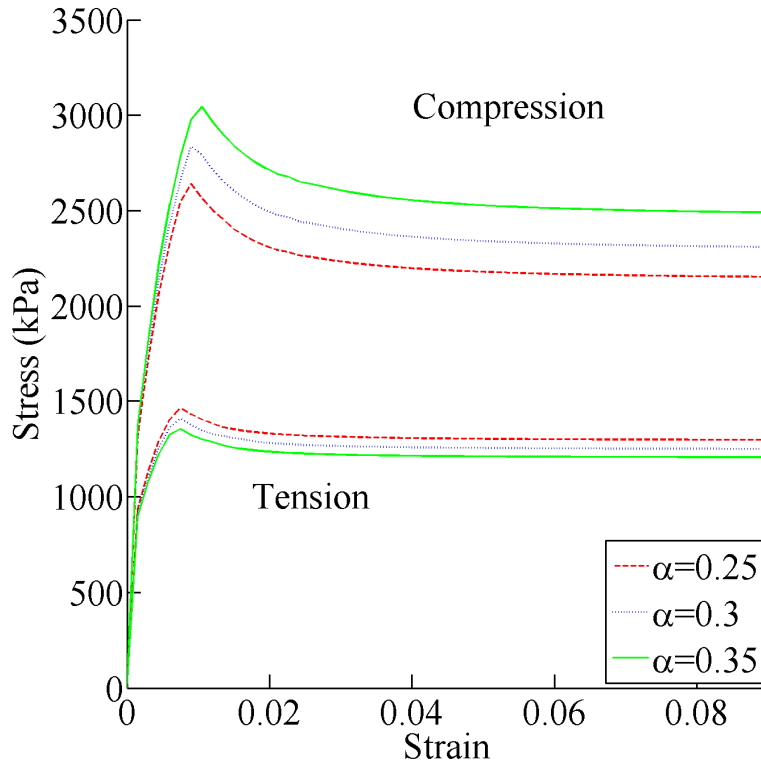


Figure 13. Effect of the damage force parameter α on the stress-strain response.

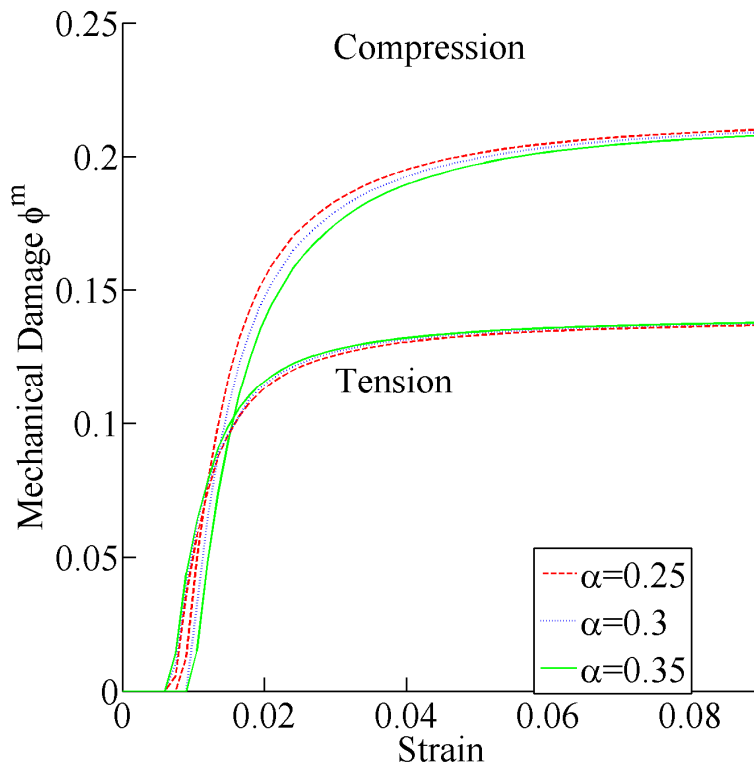


Figure 14. Effect of the damage force parameter α on the mechanical damage ϕ^m .

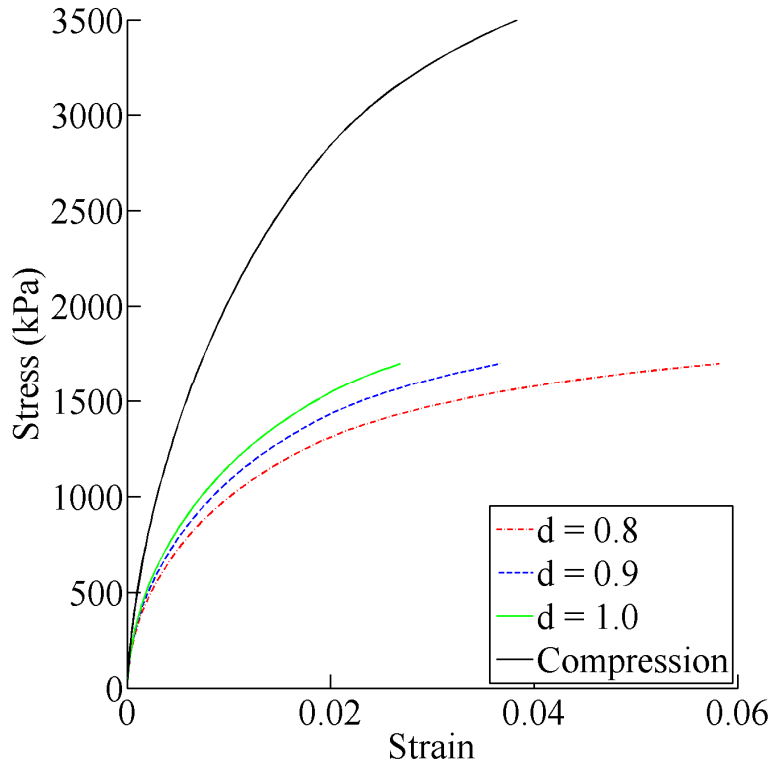


Figure 15. Effect of the damage force parameter d on the stress-strain response.

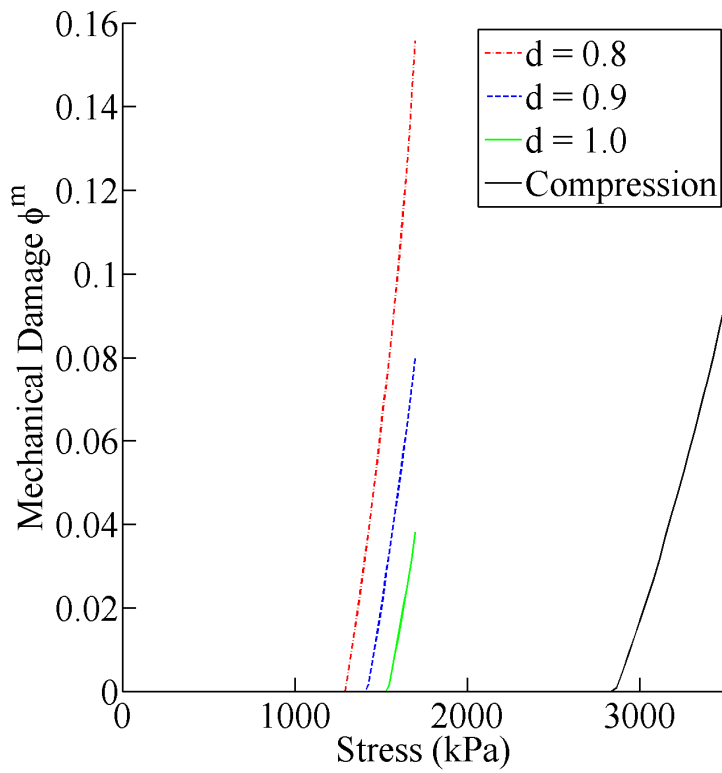


Figure 16. Effect of the damage force parameter d on the mechanical damage ϕ^m .

4 MOISTURE-INDUCED DAMAGE CONSTITUTIVE MODEL

Moisture damage contributes heavily to the premature degradation of asphalt pavements, resulting in expensive rehabilitation and replacement costs for roadways and potential hazard in the case of severely damaged roadways (Kandhal 1994, Copeland 2005, Kringos 2007). Despite the detrimental effects of moisture damage, no macroscale model exists to model moisture-induced damage in asphalt concrete mixes. The effect of moisture in degrading the mechanical properties is observed in two mechanisms: the loss of the adhesive bond between the aggregates and the mastic and the loss of the cohesive strength of the mastic (Caro et al. 2008a, Kringos et al. 2007). These mechanisms are modeled independently, but with the same method.

4.1 Damage Law

The degrading effect of moisture manifests in two physical phenomena: (1) adhesive moisture damage (corresponding to the damage variable ϕ^a), which is the degradation of the bond strength between the aggregates and the asphalt mastic due to the existence and diffusion of moisture through the thin films surrounding the aggregate particles and along the aggregate-mastic interfaces; and (2) cohesive moisture damage (corresponding to ϕ^c), which is the degradation of the cohesive strength of the asphalt mastic. In this study and for the first time, both of these phenomena are modeled independently, which allows one to introduce fundamental mechanical properties for each process (e.g., bond strength and cohesive strength) and model the transition between adhesive and cohesive damage.

The decay in the aggregate-mastic bond strength and mastic cohesive strength due to the presence of moisture is modeled using the evolution law:

$$X^i(t) = X_0^i + \int_0^t \dot{X}^i(\theta(\xi)) d\xi, \quad i = a, c \quad (36)$$

where $X^i(t)$ is the average aggregate–mastic adhesive strength of the aggregate-mastic bond for $i = a$ (adhesive) and the average mastic cohesive strength for $i = c$ (cohesive) at time t , X_0^i is the initial undamaged adhesive or cohesive strength (for $i = a, c$), and $\dot{X}^i(\theta(\xi))$ is the rate of decay of the average adhesive or cohesive strength for a normalized moisture content θ at time ξ . Time $t = 0$ is some time before moisture diffusion begins.

This evolution equation for degradation of the adhesive and cohesive strength (which will be used to describe the damage of the mix due to moisture) is an improvement over past approaches that describe the moisture-induced damage as dependent on the current state of the moisture only, not the moisture history (Kringos 2007, Kringos et al. 2007). Though some healing is observed for asphalt concrete, this is not accurately described by an instantaneous, full recovery of strength upon the change in moisture state.

For simplicity, the rate of decay $\dot{X}^i(\theta)$ is described by the linear equation:

$$\dot{X}^i(\theta(t)) = -k^i\theta(t), \quad i = a, c \quad (37)$$

where k^i ($i = a, c$) are material properties describing the rate of degradation of the adhesive or cohesive strength. Note that the k^i should be positive so that the rate of change in the strength is negative so that the value of the adhesive or cohesive strength in Eq. (36) is decreasing, i.e., degradation occurs. The units of k^i is strength per unit moisture-conditioning time. This implies that different values of k^i indicate the susceptibility of the adhesive or cohesive properties of the asphalt mixture to moisture damage such that the values of k^i can be used to rank different binders or aggregates for their susceptibility to moisture-induced damage or rank the whole mixture for moisture damage. The mixture is more susceptible to moisture damage as k^i increases.

The value of the corresponding damage variable is:

$$\phi^i = 1 - \frac{X^i(t)}{X_0^i}, \quad i = a, c \quad (38)$$

which is the simplest law that performs as expected: if the adhesive or cohesive strength is its initial value $X^i(t) = X_0^i$, there is no damage ($\phi^i = 0$) and when all adhesive or cohesive strength is lost $X^i(t) = 0$, the material is completely degraded ($\phi^i = 1$), and at intermediate values ϕ^i varies from 0 to 1.

One can write an evolution equation for the moisture-damage density by substituting Eq. (37) into the time derivative of Eq. (38), such that:

$$\dot{\phi}^i = \frac{k^i}{X_0^i}\theta(t), \quad i = a, c \quad (39)$$

Also, one can modify the above expression to include damage history such that:

$$\dot{\phi}^i = \frac{k^i}{X_0^i} \theta(t) (1 - \phi^i)^\chi, \quad i = a, c \quad (40)$$

where χ is an additional material parameter. For simplicity, Eq. (39) will be used in the following development.

In Eqs. (39) or (40), the normalized moisture content or concentration can be calculated using Fick's law for moisture diffusion:

$$\dot{\theta}(t) = D \nabla^2 \theta \quad (41)$$

where D is the diffusion coefficient and ∇^2 is the Laplacian operator. D can be a function of porosity, damage density, and temperature. However, for simplicity, in this study D is assumed to remain constant during the damage evolution.

4.2 Modified Effective Stress

In order to couple the effect of moisture-induced damage to viscoelasticity, viscoplasticity, and mechanical damage models, the effective stress concept in Eq. (28) can be redefined as follows:

$$\bar{\sigma}_{ij}(t) = \frac{\sigma_{ij}(t)}{(1 - \phi)^2} \quad (42)$$

where the total damage density, ϕ , is given by:

$$1 - \phi = (1 - \phi^m)(1 - \phi^c)(1 - \phi^a) \quad (43)$$

which includes a strong coupling between different types of damage. This will be demonstrated in the following parametric study.

4.3 Numerical Implementation

The whole model (i.e., the nonlinear viscoelastic, viscoplastic, viscodamage, and moisture damage constitutive models) is discretized and numerically implemented for displacement-based finite element simulations in the well-known commercial finite element code Abaqus (2008) using the user material subroutine UMAT.

4.3.1 Discrete viscoelastic strain

Consider the state of stress and strain at time t . At the beginning of the step, by applying the given strain increment $\Delta \boldsymbol{\varepsilon}_{ij} = \boldsymbol{\varepsilon}_{ij}^{t+\Delta t} - \boldsymbol{\varepsilon}_{ij}^t$ and knowing the values of the stress and internal variables from the previous step or time $t - \Delta t$, $(\square)^{t-\Delta t}$, the updated values at the end of the step or time t , $(\square)^t$, are obtained. Assuming small strains, we can then express:

$$\begin{aligned}\dot{\boldsymbol{\sigma}}_{ij}^t &= \dot{\boldsymbol{\sigma}}_{ij}^{ve,t} + \dot{\boldsymbol{\sigma}}_{ij}^{vp,t} = \dot{\boldsymbol{\sigma}}_{ij}^{t-\Delta t} + \Delta \dot{\boldsymbol{\sigma}}_{ij}^t = \dot{\boldsymbol{\sigma}}_{ij}^{ve,t-\Delta t} + \dot{\boldsymbol{\sigma}}_{ij}^{vp,t-\Delta t} + \Delta \dot{\boldsymbol{\sigma}}_{ij}^{ve,t} + \Delta \dot{\boldsymbol{\sigma}}_{ij}^{vp,t} \\ \dot{\boldsymbol{\sigma}}_e^{vp,t} &= \dot{\boldsymbol{\sigma}}_e^{vp,t-\Delta t} + \Delta \dot{\boldsymbol{\sigma}}_e^{vp,t} \\ \bar{\boldsymbol{\sigma}}_{ij}^t &= \bar{\boldsymbol{\sigma}}_{ij}^{t-\Delta t} + \Delta \bar{\boldsymbol{\sigma}}_{ij}^t\end{aligned}\quad (44)$$

where for some quantity x , Δx^t is the difference $x^t - x^{t-\Delta t}$. Time superscripts (\bullet^t) indicate a function is evaluated at time t .

We calculate the incremental viscoelastic shear and volumetric strains:

$$\begin{aligned}\Delta e_{ij}^t &= e_{ij}^t - e_{ij}^{t-\Delta t} \\ \Delta \dot{\boldsymbol{\sigma}}_{kk}^t &= \dot{\boldsymbol{\sigma}}_{kk}^t - \dot{\boldsymbol{\sigma}}_{kk}^{t-\Delta t}\end{aligned}\quad (45)$$

substituting in Eq. (13) for the strain to find the strains:

$$\begin{aligned}e_{ij}^{ve,t} &= \frac{1}{2} \left[g_0^t + g_1^t g_2^t \sum_{n=1}^{N_p} \bar{J}_n \left(1 - \frac{1 - \exp(-\lambda_n \Delta \psi^t)}{\lambda_n \Delta \psi^t} \right) \right] \bar{S}_{ij}^t \\ &\quad - \frac{1}{2} g_1^t \sum_{n=1}^N \bar{J}_n \left[\exp(-\lambda_n \Delta \psi^t) q_{ij,n}^{t-\Delta t} - g_2^{t-\Delta t} \frac{1 - \exp(-\lambda_n \Delta \psi^t)}{\lambda_n \Delta \psi^t} \bar{S}_{ij}^{t-\Delta t} \right] \dot{\boldsymbol{\sigma}}_{kk}^{ve,t} \\ &= \frac{1}{3} \left[g_0^t + g_1^t g_2^t \sum_{n=1}^{N_p} \bar{B}_n \left(1 - \frac{1 - \exp(-\lambda_n \Delta \psi^t)}{\lambda_n \Delta \psi^t} \right) \right] \bar{\boldsymbol{\sigma}}_{kk}^t \\ &\quad - \frac{1}{3} g_1^t \sum_{n=1}^N \bar{B}_n \left[\exp(-\lambda_n \Delta \psi^t) q_{kk,n}^{t-\Delta t} - g_2^{t-\Delta t} \frac{1 - \exp(-\lambda_n \Delta \psi^t)}{\lambda_n \Delta \psi^t} \bar{\boldsymbol{\sigma}}_{kk}^{t-\Delta t} \right]\end{aligned}\quad (46)$$

where:

$$\begin{aligned}q_{ij,n}^t &= \exp(-\lambda_n \Delta \psi^t) q_{ij,n}^{t-\Delta t} + (g_2^t \bar{S}_{ij}^t - g_2^{t-\Delta t} \bar{S}_{ij}^{t-\Delta t}) \frac{1 - \exp(-\lambda_n \Delta \psi^t)}{\lambda_n \Delta \psi^t} \\ q_{kk,n}^t &= \exp(-\lambda_n \Delta \psi^t) q_{kk,n}^{t-\Delta t} + (g_2^t \bar{\boldsymbol{\sigma}}_{kk}^t - g_2^{t-\Delta t} \bar{\boldsymbol{\sigma}}_{kk}^{t-\Delta t}) \frac{1 - \exp(-\lambda_n \Delta \psi^t)}{\lambda_n \Delta \psi^t}\end{aligned}\quad (47)$$

are the discretized shear and volumetric hereditary integrals for every Prony series term n , respectively. Those hereditary integrals are updated at the end of every converged time increment, which will be used for the next time increment.

The incremental strains, then, are:

$$\begin{aligned}
\Delta e_{ij}^t &= \hat{J}^t S_{ij}^t - \hat{J}^{t-\Delta t} \bar{S}_{ij}^{t-\Delta t} - \frac{1}{2} \sum_{n=1}^N \bar{J}_n \left[g_1^t \left(e^{-\lambda_n \Delta \psi^t} \right) - g_1^{t-\Delta t} \right] q_{ij,n}^{t-\Delta t} \\
&\quad - \frac{1}{2} g_2^{t-\Delta t} \sum_{n=1}^N \bar{J}_n \left(g_1^{t-\Delta t} \left[\frac{1 - e^{-\lambda_n \Delta \psi^{t-\Delta t}}}{\lambda_n \Delta \psi^{t-\Delta t}} \right] - g_1^t \left[\frac{1 - e^{-\lambda_n \Delta \psi^t}}{\lambda_n \Delta \psi^t} \right] \right) \bar{S}_{ij}^{t-\Delta t} \\
\Delta \dot{\sigma}_{kk}^t &= \hat{B}^t \sigma_{kk}^t - \hat{B}^{t-\Delta t} \sigma_{kk}^{t-\Delta t} - \frac{1}{2} \sum_{n=1}^N \bar{B}_n \left[g_1^t \exp(-\lambda_n \Delta \psi^t) - g_1^{t-\Delta t} \right] q_{kk,n}^{t-\Delta t} \\
&\quad - \frac{1}{3} g_2^{t-\Delta t} \sum_{n=1}^N \bar{B}_n \left(g_1^{t-\Delta t} \left[\frac{1 - e^{-\lambda_n \Delta \psi^{t-\Delta t}}}{\lambda_n \Delta \psi^{t-\Delta t}} \right] - g_1^t \left[\frac{1 - e^{-\lambda_n \Delta \psi^t}}{\lambda_n \Delta \psi^t} \right] \right) \sigma_{kk}^{t-\Delta t}
\end{aligned} \tag{48}$$

defining:

$$\begin{aligned}
\hat{J}^t &= \frac{1}{2} \left[g_0^t \bar{J}_0 + g_1^t g_2^t \sum_{n=1}^N \bar{J}_n - g_1^t g_2^t \sum_{n=1}^N \bar{J}_n \frac{1 - e^{-\lambda_n \Delta \psi^t}}{\lambda_n \Delta \psi^t} \right] \\
\hat{B}^t &= \frac{1}{3} \left[g_0^t \bar{B}_0 + g_1^t g_2^t \sum_{n=1}^N \bar{B}_n - g_1^t g_2^t \sum_{n=1}^N \bar{B}_n \frac{1 - e^{-\lambda_n \Delta \psi^t}}{\lambda_n \Delta \psi^t} \right]
\end{aligned} \tag{49}$$

4.3.2 Discrete viscoplastic strain

From Eq. (16), we approximate the incremental viscoplastic strain:

$$\Delta \dot{\sigma}_{ij}^{vp,t} = \Gamma \left(\frac{f}{\sigma_y^0} \right)^N \Delta t \frac{\partial g}{\partial \bar{\sigma}_{ij}} = \Delta \gamma^{vp,t} \frac{\partial g}{\partial \bar{\sigma}_{ij}}, \tag{50}$$

where this gives the definition of the viscoplastic multiplier $\Delta \gamma^{vp,t}$, which can be calculated discretely as:

$$\Delta \gamma^{vp,t} = \Delta t \Gamma \left(\frac{f(\bar{\sigma}_{ij}^t, \dot{\sigma}_e^{vp,t})}{\sigma_y^0} \right)^N \tag{51}$$

Substituting into Eq. (44) yields:

$$\dot{\sigma}_e^{vp,t} = \dot{\sigma}_e^{vp,t-\Delta t} + \Delta \gamma^{vp,t} \frac{\sqrt{\frac{\partial g}{\partial \bar{\sigma}_{ij}} \frac{\partial g}{\partial \bar{\sigma}_{ij}}}}{1 + 2 \left(\frac{1/2 + \beta/3}{1 - \beta/3} \right)^2} \tag{52}$$

4.3.3 Computational algorithm for the undamaged configuration

For each strain, the coupled nonlinear viscoelastic and viscoplastic algorithm starts with a trial stress (Simo and Hughes 1998) based on the nonlinear viscoelastic stress and decomposed into deviatoric and volumetric components such that their increments can be expressed as follows [see Huang et al. (2007)]:

$$\Delta S_{ij}^{t,tr} = \frac{1}{\bar{J}^{t,tr}} \left\{ \Delta e_{ij}^t + \frac{1}{2} g_1^{t,tr} \sum_{n=1}^N J_n \left[\exp(-\lambda_n \Delta \psi^t) - 1 \right] q_{ij,n}^{t-\Delta t} \right\} \quad (53)$$

$$\Delta \sigma_{kk}^{t,tr} = \frac{1}{\bar{B}^{t,tr}} \left\{ \Delta \varepsilon_{kk}^t + \frac{1}{3} g_1^{t,tr} \sum_{n=1}^N B_n \left[\exp(-\lambda_n \Delta \psi^t) - 1 \right] q_{kk,n}^{t-\Delta t} \right\} \quad (54)$$

If the trial stress exceeds the yield surface, f , the viscoplastic strain increment is calculated based on a dynamic yield surface [obtained from Eqs. (16) and (17)],

$$\chi = \bar{\tau}^{tr} - \alpha \bar{I}_1^{tr} - \kappa \left(\dot{\delta}_e^{vp,t-\Delta t} \right) - \sigma_y^0 \left(\frac{\Delta \gamma^{vp,t}}{\Gamma \Delta t} \right)^{\frac{1}{N}} \quad (55)$$

To use the Newton-Raphson root-finding algorithm, we calculate the derivative:

$$\frac{\partial \chi}{\partial \gamma^{vp}} = - \frac{\partial \kappa}{\partial \Delta \dot{\delta}_e^{vp}} \frac{\partial \Delta \dot{\delta}_e^{vp}}{\partial \gamma^{vp}} - \frac{\sigma_y^0}{N \Delta \gamma^{vp}} \left(\frac{\Delta \gamma^{vp}}{\Gamma \Delta t} \right)^{\frac{1}{N}} \quad (56)$$

where we can calculate:

$$\frac{\partial \kappa}{\partial \Delta \dot{\delta}_e^{vp}} = \frac{\partial}{\partial \Delta \dot{\delta}_e^{vp}} \kappa \left(\dot{\delta}_e^{vp,t-\Delta t} + \Delta \dot{\delta}_e^{vp,t} \right) = \kappa_1 \kappa_2 \exp \left(-\kappa_2 \left(\dot{\delta}_e^{vp,t-\Delta t} + \Delta \dot{\delta}_e^{vp,t} \right) \right)$$

and

$$\frac{\partial \Delta \dot{\delta}_e^{vp}}{\partial \gamma^{vp}} = \frac{\sqrt{\frac{\partial g}{\partial \bar{\sigma}_{ij}} \frac{\partial g}{\partial \bar{\sigma}_{ij}}}}{\sqrt{1 + 2 \left(\frac{1+\beta}{2-\frac{3}{\beta}} \right)^2}}$$

After $\partial \chi / \partial \gamma^{vp}$ is calculated, we can iterate the viscoplastic multiplier for the $k+1^{th}$ iteration:

$$\left(\Delta \gamma^{vp} \right)^{k+1} = \left(\Delta \gamma^{vp} \right)^k - \frac{\chi^k}{\left(\frac{\partial \chi}{\partial \gamma^{vp}} \right)^k} \quad (57)$$

To determine convergence, we calculate the residual strain:

$$R_{ij}^t = \Delta \dot{\delta}_{ij}^{ve,t} + \Delta \dot{\delta}_{ij}^{vp,t} - \Delta \dot{\delta}_{ij}^{ve,t} \quad (58)$$

which is the difference between the predicted strain and the actual strain (which is supplied). The trial stress for the next increment is calculated based on residual strain R_{ij}^t to be:

$$(\Delta \bar{\sigma}_{ij}^t)^{k+1} = (\Delta \bar{\sigma}_{ij}^t)^k - \left[\left(\frac{\partial R_{ij}^t}{\partial \bar{\sigma}_{kl}^t} \right)^k \right]^{-1} (R_{kl}^t)^k \quad (59)$$

where we can calculate the derivative:

$$\frac{\partial R_{ij}^t}{\partial \bar{\sigma}_{kl}^t} = \frac{\partial \dot{\delta}_{ij}^{ve,t}}{\partial \bar{\sigma}_{kl}^t} + \frac{\partial \dot{\delta}_{ij}^{vp,t}}{\partial \bar{\sigma}_{kl}^t} \quad (60)$$

where:

$$\begin{aligned} \frac{\partial \dot{\delta}_{ij}^{ve,t}}{\partial \bar{\sigma}_{kl}^t} &= \hat{J}^t \delta_{ik} \delta_{jl} + \frac{1}{3} (\hat{B}^t - \hat{J}^t) \delta_{ij} \delta_{kl} + \frac{\partial \sigma^t}{\partial \bar{\sigma}_{kl}^t} \left[\frac{\partial \hat{J}^t}{\partial \hat{\sigma}^t} + \frac{1}{3} \left(\frac{\partial \hat{B}^t}{\partial \hat{\sigma}^t} - \frac{\partial \hat{J}^t}{\partial \hat{\sigma}^t} \right) \bar{\sigma}_{kk}^t \delta_{ij} \right. \\ &\quad - \frac{1}{2} \frac{\partial g_1^t}{\partial \hat{\sigma}^t} \sum_{n=1}^{N_p} \bar{J}_n \left(e^{-\lambda_n \Delta \psi^t} q_{ij,n}^{t-\Delta t} - g_2^{t-\Delta t} \frac{1 - e^{-\lambda_n \Delta \psi^t}}{\lambda_n \Delta \psi^t} \bar{S}_{ij}^{t-\Delta t} \right) \\ &\quad - \frac{1}{2} \frac{\partial a_\sigma^t}{\partial \hat{\sigma}^t} g_1 \sum_{n=1}^{N_p} \bar{J}_n \left(e^{-\lambda_n \Delta \psi^t} \left(\frac{\lambda_n q_{ij,n}^{t-\Delta t} \Delta t}{(a_\sigma^t)^2} \bar{S}_{ij}^{t-\Delta t} + g_2^{t-\Delta t} \frac{\bar{S}_{ij}^{t-\Delta t}}{a_\sigma^t} \right) \right. \\ &\quad \left. - g_2^{t-\Delta t} \frac{1 - e^{-\lambda_n \Delta \psi^t}}{\lambda_n \Delta \psi^t} \bar{S}_{ij}^{t-\Delta t} \right) \\ &\quad - \frac{1}{9} \frac{\partial g_1^t}{\partial \hat{\sigma}^t} \sum_{n=1}^{N_p} \bar{B}_n \left(e^{-\lambda_n \Delta \psi^t} q_{kk,n}^{t-\Delta t} - g_2^{t-\Delta t} \frac{1 - e^{-\lambda_n \Delta \psi^t}}{\lambda_n \Delta \psi^t} \bar{\sigma}_{kk}^{t-\Delta t} \right) \delta_{ij} \\ &\quad - \frac{1}{9} \frac{\partial a_\sigma^t}{\partial \hat{\sigma}^t} g_1 \sum_{n=1}^{N_p} \bar{B}_n \left(e^{-\lambda_n \Delta \psi^t} \left(\frac{\lambda_n q_{kk,n}^{t-\Delta t} \Delta t}{(a_\sigma^t)^2} \bar{\sigma}_{kk}^{t-\Delta t} + g_2^{t-\Delta t} \frac{\bar{\sigma}_{kk}^{t-\Delta t}}{a_\sigma^t} \right) \right. \\ &\quad \left. - g_2^{t-\Delta t} \frac{1 - e^{-\lambda_n \Delta \psi^t}}{\lambda_n \Delta \psi^t} \bar{\sigma}_{kk}^{t-\Delta t} \right) \delta_{ij} \left. \right] \end{aligned} \quad (61)$$

(where $\hat{\sigma}$ is a scalar measure of stress which may be used for the nonlinear and shift parameters)

and:

$$\frac{\partial \dot{\delta}_{ij}^{vp,t}}{\partial \bar{\sigma}_{kl}^t} = \frac{\partial}{\partial \bar{\sigma}_{kl}^t} \left(\Delta \gamma^{vp,t} \frac{\partial g}{\partial \sigma_{ij}} \right) = \frac{\Delta t \Gamma N}{\sigma_y^0} \left(\frac{f}{\sigma_y^0} \right)^{N-1} \frac{\partial g}{\partial \sigma_{ij}} \frac{\partial f}{\partial \sigma_{kl}} + \Delta t \Gamma \left(\frac{f}{\sigma_y^0} \right)^N \frac{\partial^2 g}{\partial \sigma_{ij} \partial \sigma_{kl}} \quad (62)$$

Eq. (60) represents the viscoelastic-viscoplastic tangent stiffness. Huang (2008) and Abu Al-Rub et al. (2009) verified this numerical model as derived here and implemented using an

Abaqus user material UMAT subroutine in the commercial finite element code Abaqus (2008) by comparing it to analytical results.

4.3.4 Damage implementation

Due to adaption of the strain equivalence hypothesis in continuum damage mechanics that states that the strain in the effective (undamaged) and nominal (damaged) configurations are equal, the numerical implementation of the damage constitutive models is straightforward. The effective stress due to the undamaged nonlinear-viscoelastic–viscoplastic model calculated by the algorithm in the last section and modified according to:

$$\sigma_{ij} = (1 - \phi^a)(1 - \phi^c)(1 - \phi^m) \bar{\sigma}_{ij}, \quad (63)$$

where each ϕ is calculated at each time step.

Mechanical damage is calculated using the effective stress in the undamaged configuration. Hence, once the updated effective stress increment is calculated [Eq. (59)], the total effective stress is calculated. Then, one can calculate the final viscoelastic and viscoplastic strains. Therefore, once the updated effective stress and strain tensors are calculated, one can check if damage have initiated or not using Eq. (30). If damage is initiated, then one can calculate the rate of the mechanical damage density using Eq. (34) such that:

$$\dot{\phi}^t = \dot{\phi}^{t-\Delta t} + \dot{\phi}^t \Delta t \quad (64)$$

For the moisture damage variables, the evolution integral Eq. (36) is discretized (substituting the material law Eq. (37) to be:

$$X^{i,t} = X^{i,t-\Delta t} - k^i \theta^t \Delta t, \quad i = a, c \quad (65)$$

with an initial value of the initial adhesive or cohesive strength:

$$X^{i,t=0} = X_0^i, \quad i = a, c \quad (66)$$

indicating a material initially undamaged by moisture. The moisture damage variables ϕ^a and ϕ^c may be computed directly from Eq. (38). See Figure 17 for the numerical algorithm.

Abaqus stress–temperature elements are used for finite element simulations, where the temperature variable represents the normalized moisture content, θ , recognizing that Fick’s moisture diffusion and Fourier’s heat flow laws are analogous. The diffusion coefficient D for hot mix asphalt was determined by Kassem (2006).

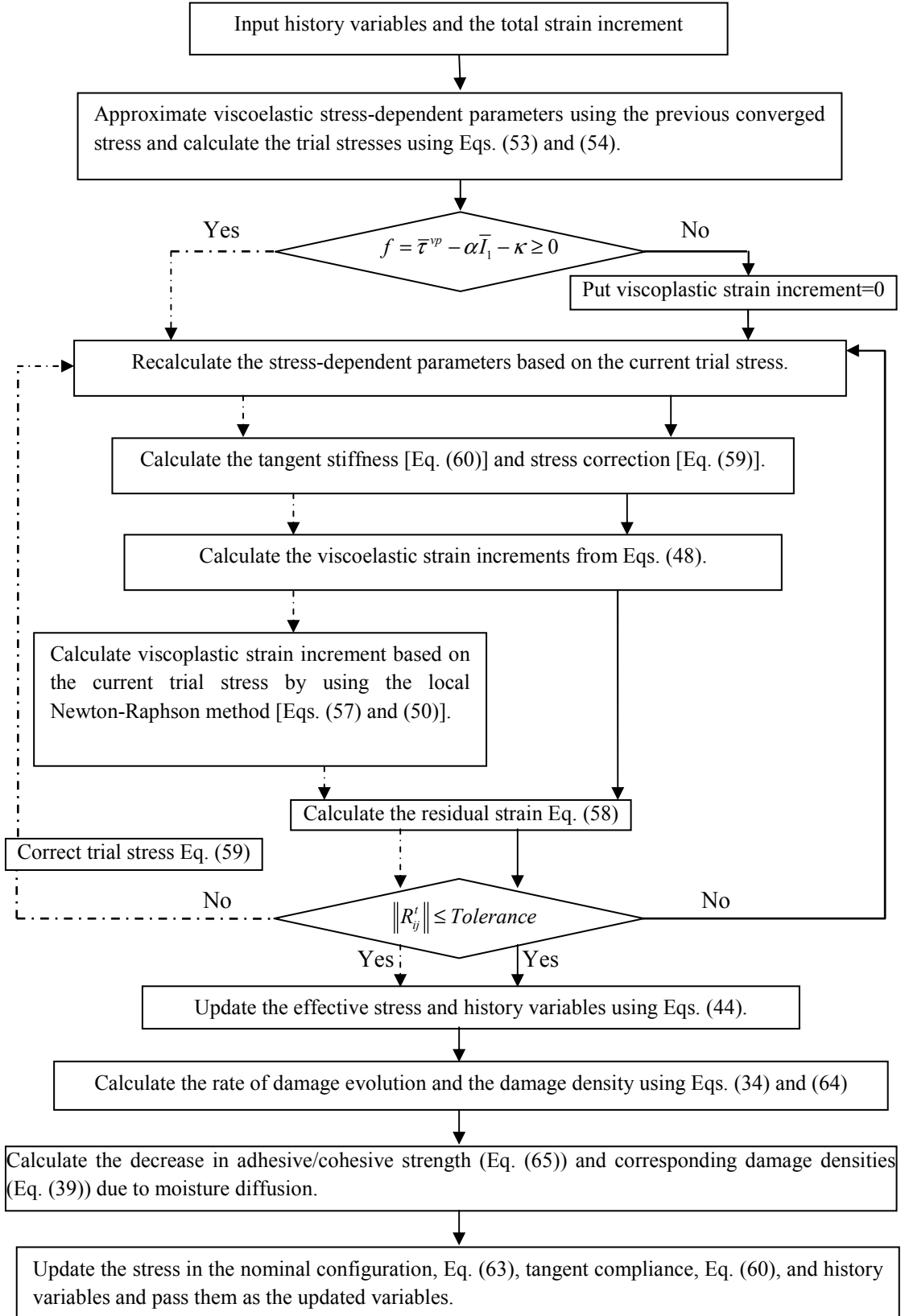


Figure 17. Flowchart for numerical implementation of the proposed constitutive model.

4.4 Simulation Results from Moisture-Induced Damage Modeling

4.4.1 Moisture damage–mechanical damage coupling

It is expected that a material will become more susceptible to mechanical damage due to moisture exposure, and since there are no special laws postulated for coupling mechanical and moisture damage, it is not instantly clear whether this coupling is described by the damage model presented here. In fact, intrinsic (or implicit) coupling exists due to stress-controlled loading, but not strain-controlled loading, because the mechanical damage is driven by the effective stress $\bar{\sigma}_{ij}$ (recall Eq. (29)). Thus, in the presence of moisture damage an applied stress is amplified (Eq. (28)) to calculate the damage driving force, but in the case of strain-controlled damage, the effective stress is calculated due to the strain, which does not change because of the formulation $\dot{\sigma} = \bar{\sigma}_{ij}$ (Eq. (6)).

To illustrate this coupling, several simulations were performed with constant stress rate loading after moisture exposure at various levels. To isolate damage effects, the material law used is elastic–damaged, with material properties Young’s modulus $E = 100 \text{ MPa}$, $Y_{th}^m = 2 \text{ MPa}$, $k^m = 0.1$, $X_0^a = 100.0$, $k^a = 0.01$, and $k^c = 0$. The material is subjected to the specified moisture level for 2000 seconds before loading in tension at stress rate $\dot{\sigma} = 10 \text{ MPa / s}$.

Figure 18 plots the resulting stress–strain diagrams, showing the greater the moisture exposure, the weaker the material is, and that this weakening is more than proportional to the moisture effects. Figure 19 plots the evolution of the total damage variable ϕ . Before time $t = 2000$ seconds there is no mechanical loading, so all of the damage is due to moisture. Sometime after mechanical loading starts, mechanical damage accumulates in all of the samples, with earlier onset and greater growth of the damage for greater moisture exposure. Figure 20 shows the evolution of the mechanical damage variable ϕ^m alone to emphasize the differences between the mechanical damage in simulations with the same mechanical loading and different moisture loading. It is clear from these figures that the predictions qualitatively agree with experimental observations and the obvious. The damage onset decreases as moisture loading increases. Moreover, from Figure 18, it is obvious that the moisture loading affects the initial response (elastic or viscoelastic).

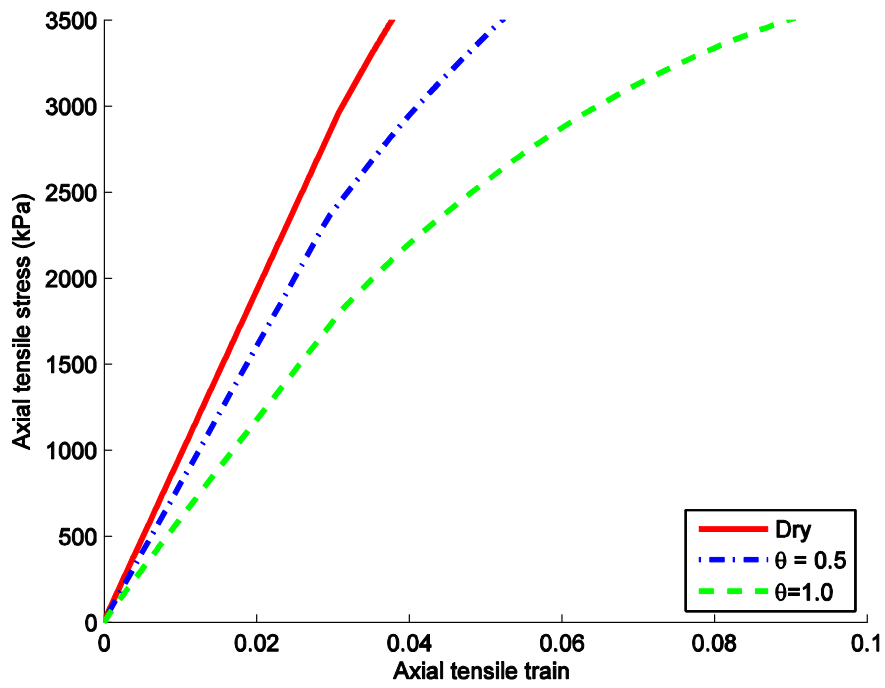


Figure 18. Stress–strain diagrams due to stress-controlled loads for various moisture exposures.

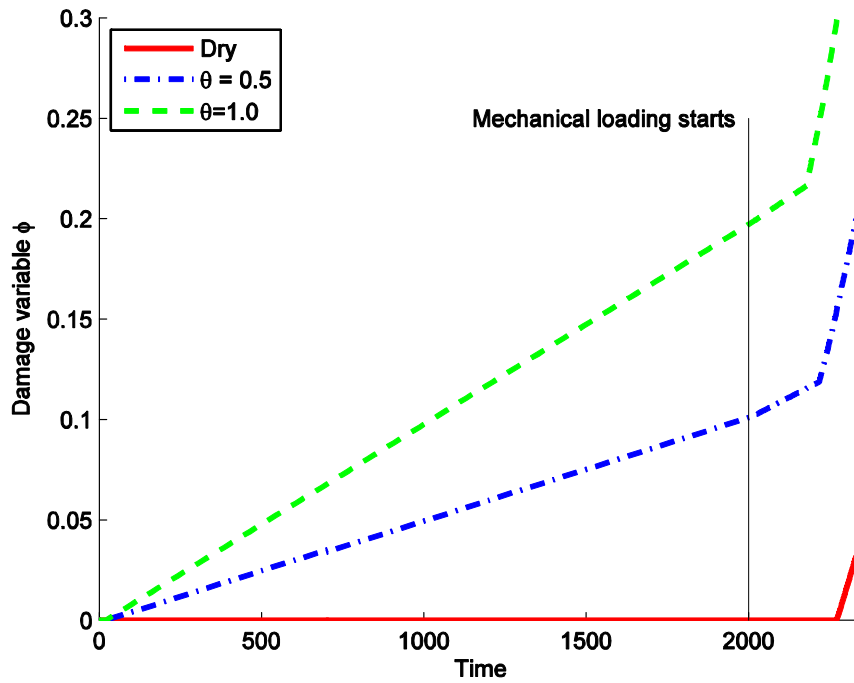


Figure 19. The evolution of damage variable ϕ due to stress-controlled loads with time for various moisture exposures.

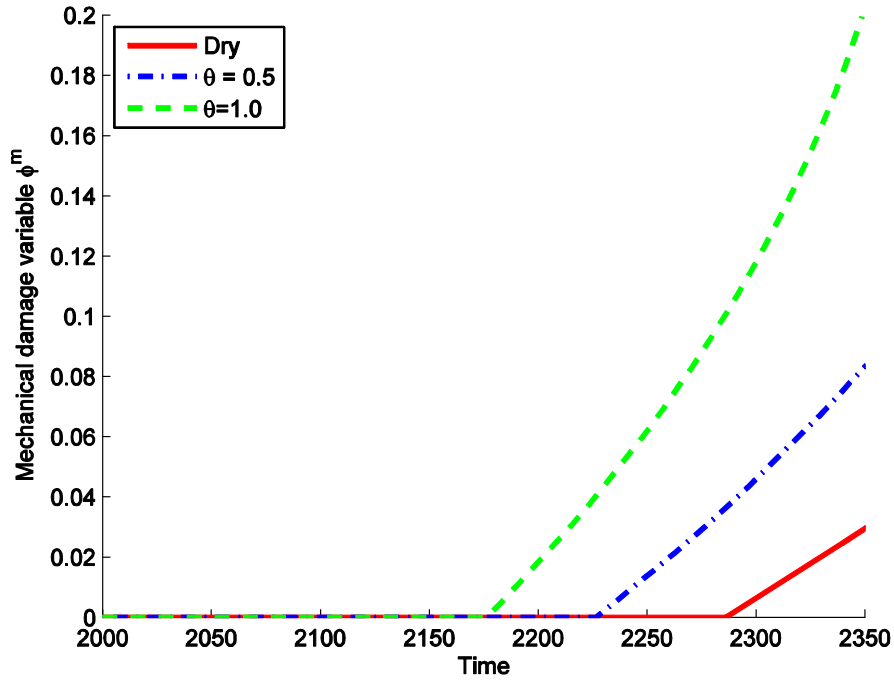


Figure 20. The evolution of mechanical damage variable ϕ^m due to stress-controlled loads with time for various moisture exposures.

4.4.2 Viscoelastic–viscoplastic–mechanical damage–moisture damage model

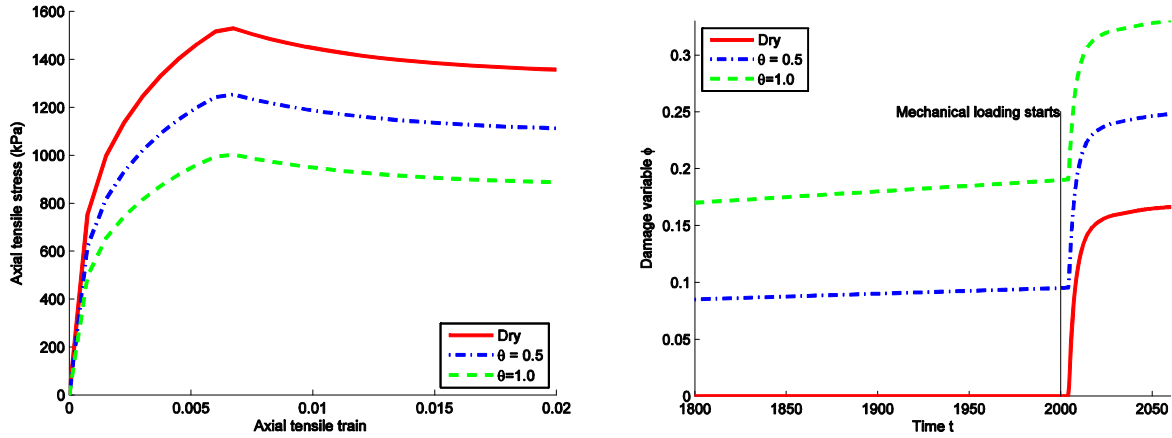
Several simulations' results show the function of the complete constitutive model, featuring viscoelasticity, viscoplasticity, mechanical damage, and moisture damage. The mechanical damage material parameters are as reported in past sections, and the moisture damage parameters are as follows: $X_0^a = 100.0$, $k^a = 0.01$, and $k^c = 0$ (i.e., there is no cohesive moisture damage). Table 2 lists the viscoelastic and viscoplastic material parameters.

4.4.2.1 Constant strain rate simulations

Figure 21 shows the results of constant strain rate tests with different moisture exposures. The normalized moisture content θ is held constant for 2000s and then the material is loaded at constant strain rate $\dot{\delta} = 0.0015\text{s}^{-1}$. Note the effect of moisture damage, causing the material to become weaker and less stiff. Damage grows due to the presence of moisture and accelerates due to mechanical loading.

Table 2. Viscoelastic and viscoplastic material parameters.

n	$\lambda_n(1/s)$	$J_n(1/kPa)$	Property	Value
1	1.0	1.15×10^{-6}	α	0.3
2	0.1	1.49×10^{-6}	d	0.9
3	0.01	3.17×10^{-6}	σ_y^0	35kPa
4	0.001	6.37×10^{-6}	β	0.25
5	0.0001	2.61×10^{-6}	Γ	$5 \times 10^{-7} s^{-1}$
6	0.00001	96.1×10^{-6}	N	2.0
J_0	—	0.675×10^{-6}	κ_0	35kPa
$g_o = g_1 = g_2$	—	1.0	κ_1	600kPa
			κ_2	290

**Figure 21.** Stress–strain and damage evolution plots for constant uniaxial strain rate simulations for several moisture conditioning levels.

4.4.2.2 Constant stress rate simulations

Figure 22 shows the stress–strain curves for constant compressive stress rate simulations with different moisture levels. The material is subjected to the moisture content specified for 2000 seconds and then subjected to a compressive stress at constant rate $\dot{\sigma} = 10 \text{ kPa} / \text{s}$.

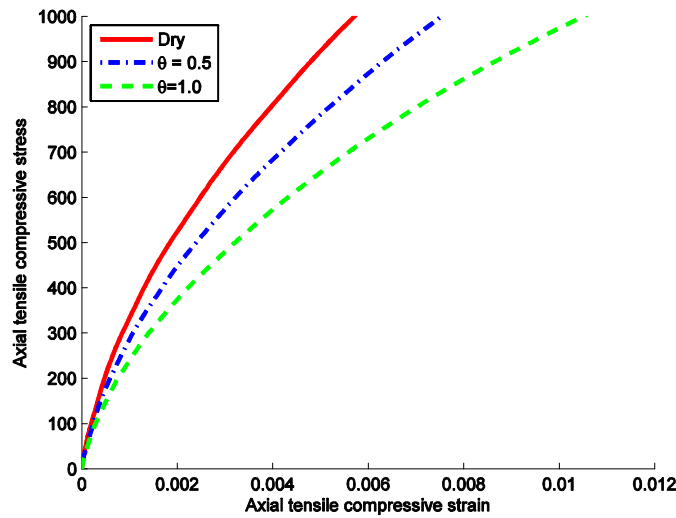


Figure 22. Stress–strain diagrams for constant uniaxial stress rate simulations for several moisture conditioning levels.

4.4.2.3 Creep–recovery simulations

Figure 23 shows the strain response due to constant tensile stress $\sigma = 500\text{ kPa}$ for 50 seconds then allowed to recover with the load removed for 50 seconds, all after 2000 seconds of moisture exposure at various levels.

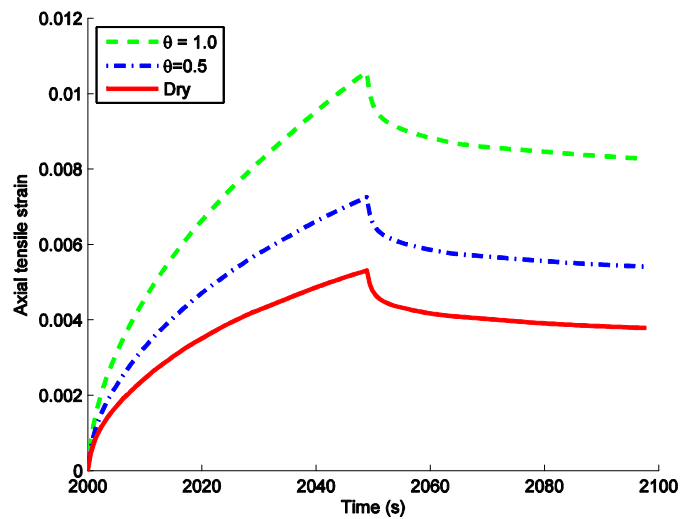


Figure 23. Strain vs. time for tensile creep–recovery simulations for several moisture conditioning levels.

4.4.3 Micromechanical simulations

Continuum models are fundamentally incapable of describing effects that are occurring at a scale smaller than continuity is imposed. The effects of composition and geometry at a microscale in asphalt concrete mixes lead to their continuum properties. Micromechanical modeling is beyond the scope of this study, but a few simulations are performed and their results presented here to show the model's fitness for micromechanical computational modeling.

Though the material model presented in this study is developed to model asphalt concrete mixes as continua, it is extremely well-suited to asphalt mastic, which exhibits time-dependent recoverable and irrecoverable deformations, and degrades with loading and moisture exposure. The response of aggregates is usually very stiff and time-table, and may be modeled with a simple linear elastic material law. (Recent work by Luo and Lytton (2009) suggests a viscoelastic law might be more appropriate for aggregates, possibly due to binder absorption in the aggregates. This or any other accessible material model for aggregate would also be simple to incorporate in a finite element simulation if necessary.)

For these simulations, finite element meshes were constructed with three types of regions: aggregates, asphalt mastic bulk, and asphalt mastic in the aggregate–mastic bond region and all are given different material properties. For simplicity, the aggregates are assumed to have a circular shape. Furthermore, the aggregates are modeled as isotropic linear elastic material with Young's modulus $E_{\text{agg}} = 1\text{GPa}$ and Poisson's ratio $\nu_{\text{agg}} = 0.16$. For the mastic, $X_0^a = 100$, $X_0^c = 100$, $k^c = 0.01$, and $k^a = 0.02$ in the adhesive zones and $k^a = 0$ outside the cohesive zones. The normalized diffusivities for the mastic and aggregate are $10^{-5} \text{m}^2\text{s}^{-1}$ and $10^{-10} \text{m}^2\text{s}^{-1}$, respectively. Plane-strain linear finite elements simulations are conducted.

4.4.3.1 Dry simulations

Figure 24 and Figure 25 are contour plots showing the distribution of stress and damage due to compressive loading at constant average strain rate $\dot{\epsilon} = 0.0015\text{s}^{-1}$, and through the simulation, the geometry of the body causes stress to concentrate in some parts of the mesh. When the stress becomes very high, the material sustains damage, and becomes less stiff. Corresponding to this loss in stiffness, the formerly high-stress material 'attracts' less load, and the areas with high deformation have small values of stress in Figure 24 and high values of damage in Figure 25.

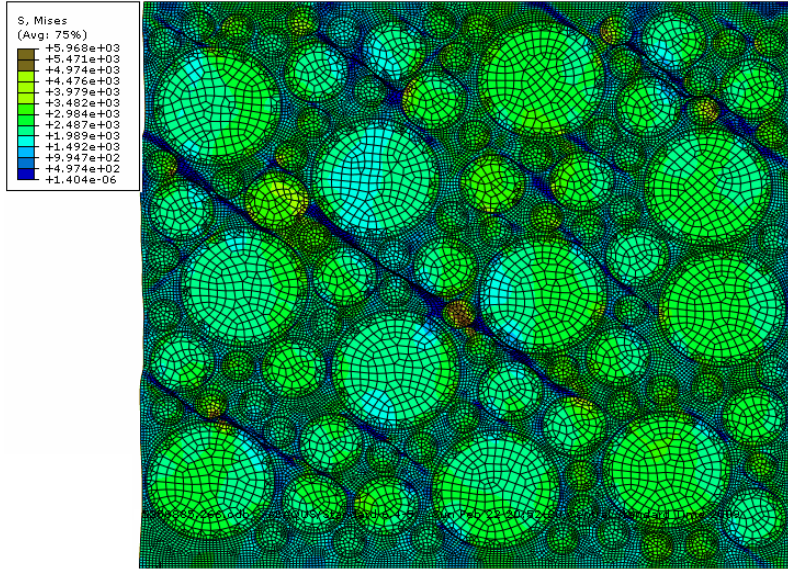


Figure 24. Von Mises stress distribution due to compressive loading with no moisture exposure.

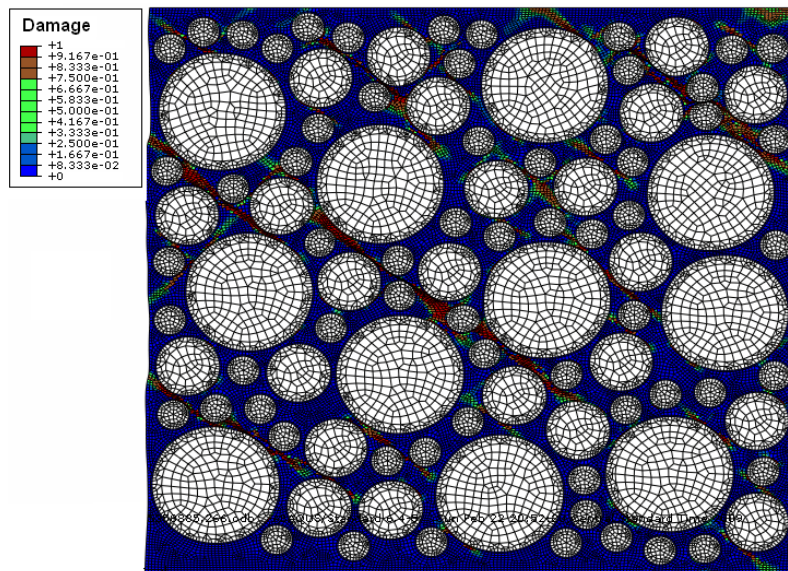


Figure 25. Damage variable distribution due to compressive loading with no moisture exposure.

4.4.3.2 Moisture-affected simulations

Several figures show the result of a simulation featuring both moisture and mechanical loading. The body is subjected to constant normalized moisture content $\theta = 1.0$ on its top edge and $\theta = 0.0$ on its bottom edge for 2000 seconds before being loaded in compression at constant average strain rate $\dot{\delta} = 0.0015 s^{-1}$. Figure 26 shows the final moisture distribution, which leads to the moisture-induced damage.

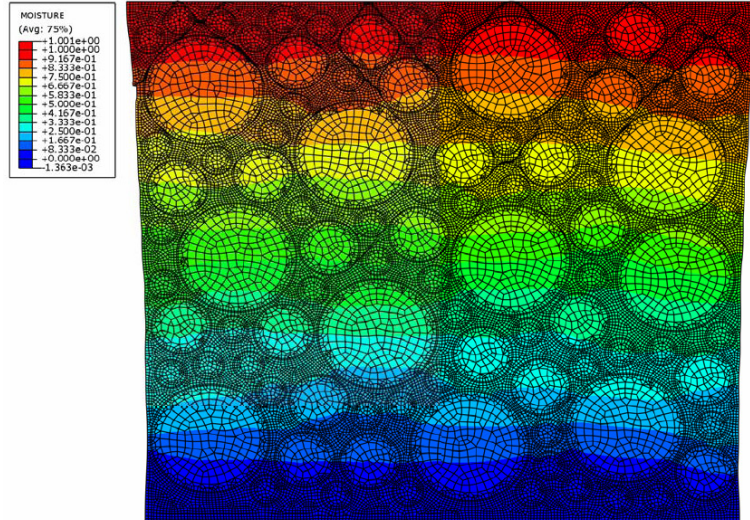


Figure 26. Final moisture distribution.

Figure 27 depicts the stress distribution after some mechanical loading; stress is concentrated due to geometry and moisture damage effects. Figure 28 is the total damage distribution due to mechanical loading after moisture exposure; compare Figure 28 to Figure 25: the degrading presence of moisture has greatly changed the damage's location and distribution. Figure 25 shows large, continuous damaged regions (cracking) whereas the moisture-exposed body in Figure 28 shows more compact, isolated, concentrated damaged regions surrounding the aggregates (raveling).

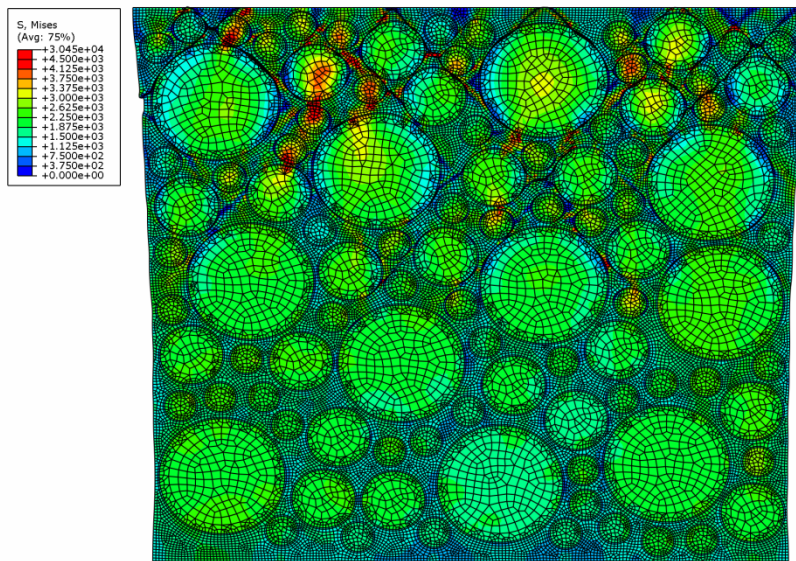


Figure 27. Von Mises stress distribution due to moisture exposure followed by compressive loading.

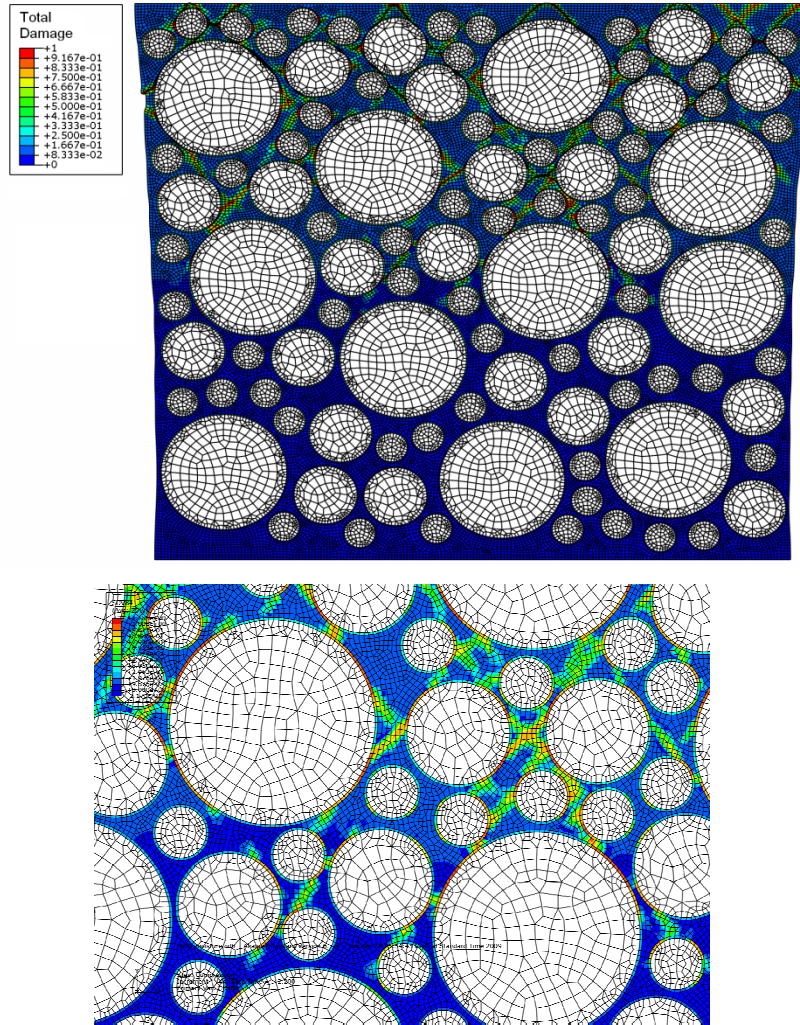


Figure 28. Total damage distribution due to moisture exposure followed by compressive loading. The inset shows adhesive moisture-induced damage.

Figure 27 and Figure 28 show that the model performs as expected: moisture-induced damage occurs to a greater degree in the areas closer to moisture-exposed surfaces. The loss of strength at the aggregate-mastic interface in particular is severe, and the interface zone attracts much of the degradation as seen by the total damage.

Figure 29 is the average stress–average strain diagram for the body, plotted for the moisture damaged body and for dry material. The composite stiffness and ultimate strength are reduced in the moisture-exposed case, which agrees well with experimental observations.

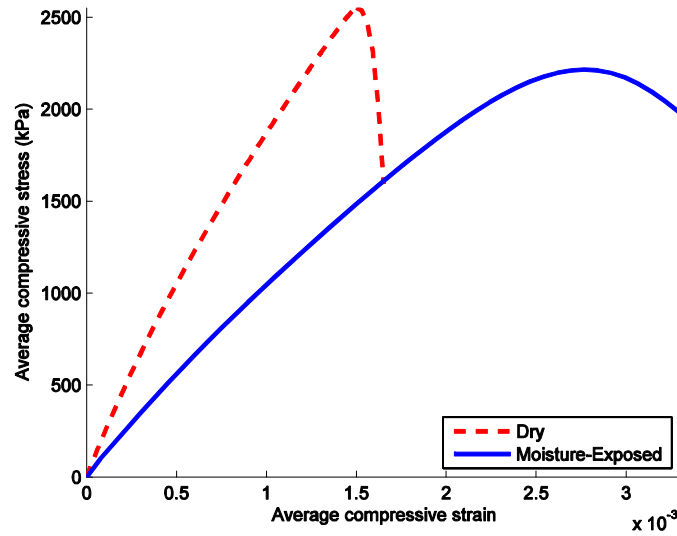


Figure 29. Load–displacement (average stress versus average strain) diagrams for compressive loading with and without moisture exposure.

The results from the micromechanical simulations show that the mechanical/moisture damaged nonlinear-viscoelastic–viscoplastic material model presented in this study is well-suited to microscale simulations of asphalt concrete. Future studies can use this model with experimentally-determined material parameters for the constituents to predict the bulk response of asphalt concrete.

5 CONCLUSIONS

5.1 Summary

The presented model captures the whole mechanical response of an asphalt mix subjected to mechanical and moisture loads using a continuum model. The nonlinear viscoelastic character of the reversible deformations is modeled using Schapery's theory. The viscoplastic character of the rate-dependent permanent deformations is modeled using Perzyna viscoplasticity, with a modified Drucker–Prager yield surface used to capture the dependence on state of stress anticipated for asphalt concrete and with a non-associated flow rule to describe the appropriate volumetric viscoplastic response.

Damage is described due to extreme mechanical loads and due to moisture. The mechanically-induced damage model predicts degradation due to the same modified Drucker–Prager surface used for viscoplasticity with an exponential damage evolution function. Rate-dependence of mechanical damage is presented and a basic adaptation of the model is provided. Moisture-induced damage is treated realistically as two mechanisms: degradation of the adhesive bond between the mastic and aggregates and degradation of the cohesive strength of the mastic. The moisture-induced damage model is formulated in a novel way, accounting for the gradual, irreversible degradation of a mix using continuum damage mechanics.

This model is the first continuum model to capture all facets of realistic asphalt mix response, as described. One major simplification within the proposed model is anisotropy; all effects are assumed to be isotropic. In the case of moisture-induced damage this may be realistic, but it is at least somewhat unphysical in the mechanical laws. This assumption is made to keep from overcomplicating the model, and can be relaxed if experiments show anisotropy effects are important.

The nonlinear-viscoelastic–viscoplastic–damage model is implemented numerically for solving 3D and 2D plane strain problems with arbitrary geometries in the finite element method, using a UMAT user subroutine for the finite element code Abaqus (2008). The presented simulation results show the meaning and effect of the various material parameters governing the nonlinear viscoelastic, viscoplastic, and damage behavior in the parametric studies, and show the predicted response for various simulated tests to match the qualitative behavior to experiments.

The current moisture-induced damage model is simple and easy to use by pavement engineers to predict the time frame over which moisture-induced damage may occur under different environmental and traffic loading conditions. This computational tool will give highway agencies and contractors the ability to easily perform “what-if” scenarios for asphaltic pavements, tweaking mix designs and compositions for maximum performance while producing quality asphalt mix in compliance with required specifications. Therefore, the proposed model, which is developed based on fundamental moisture-induced damage mechanisms, can be used for predicting moisture-induced damage as a durability indicator and to modify mix composition that increases durability and minimizes the risk of failure. Lowering the risk translates to lower cost to the highway agency and the public, reduce maintenance operations, and extending the pavement’s service life.

5.2 Future Work

Fitting experimental data to the model is a nontrivial task, due to the large number of material parameters and their inter-coupling in tests. Work is currently underway at Texas A&M University to develop a systematic way to fit all material parameters in the proposed model for a given asphalt mix. Moreover, the authors are currently conducting novel pull-off tests on aggregate-mastic specimens that are subjected to various moisture-conditioning times. The results from these experiments can be used for calibrating the adhesive and cohesive moisture-damage evolution laws. Finally, a comprehensive moisture-induced damage experiments on several asphalt mixtures will be conducted under different loading conditions that will be used for further validation and verification of the current proposed constitutive equations.

REFERENCES

- Abaqus (2008). *Version 6.8*, Habbit, Karlsson and Sorensen, Inc, Providence, RI.
- Abu Al-Rub, R.K., Voyiadjis, G.: On the coupling of anisotropic damage and plasticity models for ductile materials. *International Journal of Solids and Structures* **40**, 2611–2643 (2003).
- Abu Al-Rub, R.K., Voyiadjis, G.: Gradient-enhanced coupled plasticity-anisotropic damage model for concrete fracture: computational aspects and applications. *International Journal of Damage Mechanics* (2009).
- Abu Al-Rub, R.K., Masad, E.A., Huang, C.W.: Improving the sustainability of asphalt pavements through developing a predictive model with fundamental material properties. Final Report submitted to Southwest University Transportation Center, Report # SWUTC/08/476660-0007-1 (2009).
- Airey, G., Rahimzadeh, B., Collop, A.C.: Linear viscoelastic limits of bituminous binders. *Journal of Associated Asphalt Paving Technologists* **17**, 89–115 (2002a).
- Airey, G., Rahimzadeh, B., Collop, A.C.: Viscoelastic linearity limits for bituminous materials. *Materials and Structures* **36**(10), 643–647 (2002b).
- Airey, G., Rahimzadeh, B., Collop, A.C.: Linear rheological behavior of bituminous paving material. *Journal of Materials in Civil Engineering* **16**, 212–220 (2004).
- ASTM: Standard test method for indirect tension test for resilient modulus of bituminous mixtures. In: E 380-91a. ASTM International, West Conshohocken, PA (1995). Test Procedure D.
- Bhasin, A.: Development of methods to quantify bitumen-aggregate adhesion and loss of adhesion due to water. PhD dissertation, Texas A&M University, College Station, Texas (2006).
- Bhasin, A., Masad, E., Little, D., Lytton, R.: Limits on adhesive bond energy for improved resistance of hot mix asphalt to moisture damage. *Transportation Research Record* **1970**, 3–13 (2006).
- Caro, S., Masad, E., Bhasin, A., Little, D.: Moisture susceptibility of asphalt mixtures, Part 1: Mechanisms. *International Journal of Pavement Engineering* **9**, 81–98 (2008a).

- Caro, S., Masad, E., Bhasin, A., Little, D.: Moisture susceptibility of asphalt mixtures, Part 2: Characterisation and modeling. *International Journal of Pavement Engineering* **9**, 99–114 (2008b).
- Chehab, G., Kim, Y.R., Schapery, R., Witzczak, M., Bonaquist, R.: Characterization of asphalt concrete in uniaxial tension using a viscoelastoplastic model. *Journal of Associated Asphalt Paving Technologists* **72**, 326–370 (2003).
- Chen, J., Lin, K., Young, S.: Effects of crack width and permeability on moisture-induced damage of pavements. *Journal in Materials in Civil Engineering* **16**(3), 276–282 (2006).
- Cheung, C., Cebon, D.: Deformation mechanisms of pure bitumen. *Journal of Materials in Civil Engineering* **9**, 117–129 (1997).
- Chiarelli, A., Shao, J., Hoteit, N.: Modeling of elastoplastic damage behavior of a claystone. *International Journal of Plasticity* **19**(1), 23–45 (2003). DOI 10.1016/S0749-6419(01)00017-1.
- Cicekli, U., Voyiadjis, G., Abu Al-Rub, R.K.: A plasticity and anisotropic damage model for plain concrete. *International Journal of Plasticity* **23**(10–11), 1874—1900 (2007).
- Collop, A., Scarpas, A., Kasbergen, C., de Bondt, A.: Development and finite element implementation of stress-dependent elastoviscoplastic constitutive model with damage for asphalt. *Transportation Research Record* **1832**, 96–104 (2003).
- Copeland, A.: Moisture in asphalt pavements in the United States: A financial perspective. First International Workshop on Moisture Damage (2005).
- Darabi, M.K., Abu Al-Rub, R.K., Masad, E.A., Huang, C.-W., Little, D.N.: A thermo-viscoelastic-viscoplastic-viscodamage constitutive model for asphaltic materials. *International Journal of Solids and Structures* 2010 (in press).
- Dessouky, S.: Multiscale approach for modeling hot mix asphalt. PhD dissertation, Texas A&M University, College Station, Texas (2005).
- Di Benedetto, H., Mondher, N., Sauzeat, C., Olard, F.: Three-dimensional thermo-viscoplastic behavior of bituminous materials. *Road Material Pavement* **8**, 285–316 (2007)
- Field, F., Phang, W.: Stripping in asphaltic concrete mixes, observations and test procedures. *Canadian Technical Asphalt Association* **12**, 61–68 (1967).

- Grenfell, J., Collop, A., Airey, G., Taherkhani, H., Scarpas, A.T.: Deformation characterisation of asphalt concrete behaviour. In: Proceedings of the AAPT 2008, pp. 1–34. Engineers' Soc. of Western Pennsylvania, Philadelphia, USA (2008).
- Ha, K., Schapery, R.: A three-dimensional viscoelastic constitutive model for particulate composites with growing damage and its experimental validation. *International Journal of Solids and Structures* **35**(26–27), 3497–3517 (1998). DOI 10.1016/S0020-7683(97)00213-8.
- Haj-Ali, R.M., Muliana, A.H.: Numerical finite element formulation of the Schapery nonlinear viscoelastic material model. *International Journal of Numerical Methods in Engineering* **59**(1), 25–45 (2004).
- Huang, C.W.: Development and numerical implementation of nonlinear viscoelastic–viscoplastic model for asphalt materials. PhD dissertation, Texas A&M University, College Station, Texas (2008).
- Huang, C.W., Masad, E., Muliana, A.H., Bahia, H.: Nonlinearly viscoelastic analysis of asphalt mixes subjected to shear loading. *Mechanics of Time-Dependent Materials* **22**, 91–110 (2007).
- Kachanov, L.: On the creep fracture time. *Izv Akad, Nauk USSR Otd. Tech.* **8**, 26–31 (1958).
- Kachanov, L.: A simple technique of stress analysis in elastic solids with many cracks. *International Journal of Fracture* **28**, R11–19 (1985).
- Kandhal, P.: Field and lab investigation of stripping in asphalt pavements: State-of-the-art. *Transportation Research Record* **1454** (1994).
- Kassem, E.A.R.: Measurements of moisture suction in hot mix asphalt mixes. MS thesis, Texas A&M University, College Station, Texas (2006).
- Kassem, E.A.R.: Compaction effects on uniformity, moisture diffusion, and mechanical properties of asphalt pavements. PhD dissertation, Texas A&M University, College Station, Texas (2008).
- Kringos, N.: Modeling of combined physical-mechanical moisture induced damage in asphaltic mixes. PhD dissertation, Delft University, Delft, The Netherlands (2007).
- Kringos, N., Scarpas, A.T.: Raveling of asphaltic mixes due to water damage: Computational identification of controlling parameters. *Transportation Research Record* **1929**, 79–87 (2005).

- Kringos, N., Scarpas, A.T.: Physical and mechanical moisture susceptibility of asphaltic mixtures. *International Journal of Solids and Structures* **45**, 2671–2685 (2007).
- Kringos, N., Scarpas, A.T.: Physical and mechanical moisture susceptibility of asphaltic mixtures. *International Journal of Solids and Structures* **45**, 2671–2685 (2008).
- Kringos, N., Scarpas, A.T., Copeland, A., Youtcheff, J.: Modeling of combined physical-mechanical moisture induced damage in asphaltic mixes – Part 2: moisture susceptibility parameters. *International Journal for Pavement Engineering* **9**, 129–151 (2008a).
- Kringos, N., Scarpas, A.T., Kasbergen, C.: Three dimensional elasto-viscoplastic finite element model for combined physical-mechanical moisture induced damage in asphaltic mixes. *Journal of Associated Asphalt Paving Technologists* **76**, 495–524 (2007).
- Kringos, N., Scarpas, A.T., Kasbergen, C., Selvadurai, A.: Modeling of combined physical-mechanical moisture induced damage in asphaltic mixes – Part 1: governing processes and formulations. *International Journal for Pavement Engineering* **9**, 115–128 (2008b).
- Lemaitre, J.: *Engineering Damage Mechanics: Ductile, Creep, Fatigue and Brittle Failures*. Springer, Berlin Heidelberg (2005). DOI 10.1007/b138882.
- Lemaitre, J., Chaboche, J.L.: *Mechanics of Solid Materials*. Cambridge University Press, London (1990).
- Levenberg, E., Uzan, J.: Triaxial small-strain viscoelastic-viscoplastic modeling of asphalt aggregate mixes. *Mechanics of Time-Dependent Materials* **8**(4), 365–384 (2004).
- Little, D., Jones, D.: Chemical and mechanical mechanisms of moisture damage in hot mix asphalt pavements. *Moisture Sensitivity of Asphalt Pavements: A National Seminar* pp. 713–754 (2003).
- Lu, Y., Wright, P.J.: Numerical approach of visco-elastoplastic analysis for asphalt mixtures. *Journal of Computers and Structures* **69**, 139–157 (1998).
- Luo, R., Lytton, R.L.: Self-consistent micromechanics models of an asphalt mixture. *Transportation Research Board 2009 Annual Meeting CD-ROM* pp. 1–17 (2009).
- Lytton, R., Masad, E., Zollinger, C., Bulut, R., Little, D.: Measurements of surface energy and its relationship to moisture damage. *Technical Report FHWA/TX-05/0-4524-2*, Texas Transportation Institute, College Station, Texas (2005).
- Masad, E., Al-Omari, A., Lytton, R.: A simple method for predicting laboratory and field permeability of hot mix asphalt. *Transportation Research Record* **1970**, 55–63 (2006a).

- Masad, E., Castelblanco, A., Birgisson, B.: Effects of air void size distribution, pore pressure, and bond energy on moisture damage. *Journal of Testing and Evaluation* **34**(1), 1–9 (2006b).
- Masad, E., Dessouky, S., Little, D.: Development of an elastoviscoplastic microstructural-based continuum model to predict permanent deformation in hot mix asphalt. *International Journal of Geomechanics* **7**, 119–130 (2007a).
- Masad, E., Huang, C.W., Airey, G., Muliana, A.: Nonlinear viscoelastic analysis of unaged and aged asphalt binders. *Construction and Building Materials* **22**, 2170–2179 (2007b).
- Masad, E., Zollinger, C., Bulut, R., Little, D., Lytton, R.: Characterization of HMA moisture damage using surface energy and fracture properties. *Journal of the Association of Asphalt Paving Technologists* **75**, 713–754 (2006c).
- Nicholson, V.: Adhesion tension in asphalt pavements, its significance and methods applicable in its determination. *Journal of the Association of Asphalt Paving Technologists* **3**, 28–48 (1932).
- Oeser, M., Moller, B.: 3d constitutive model for asphalt pavements. *International Journal of Pavement Engineering* **5**, 153–161 (2004).
- Park, S., Schapery, R.: A viscoelastic constitutive model for particulate composites with growing damage. *International Journal of Solids and Structures* **34**(8), 931–947 (1997).
- Park, S.W., Kim, Y.R., Schapery, R.A.: A viscoelastic continuum damage model and its application to uniaxial behavior of asphalt concrete. *Mechanics of Materials* **24**(4), 241–255 (1996).
- Perl, M., Uzan, J., Sides, A.: Visco-elasto-plastic constitutive law for bituminous mixture under repeated loading. *Transportation Research Record* **911**, 20–26 (1983).
- Perzyna, P.: The constitutive equations for rate-sensitive materials. *Quarterly of Applied Mathematics* **20**, 321–332 (1963).
- Perzyna, P.: Fundamental problems in visco-plasticity. In: *Advances in Applied Mechanics*, vol. 9, pp. 243–377. Academic Press, New York (1966).
- Perzyna, P.: Thermodynamic theory of viscoplasticity. In: *Advances in Applied Mechanics*, vol. 11, pp. 313–354. Academic Press, New York (1971).
- Roels, S., Moonen, P., Proft, K.D., Carmeliet, J.: A coupled discrete-continuum approach to simulate moisture effects on damage processes in porous materials. *Computer Methods in Applied Mechanics and Engineering* **195**(52), 7139–7153 (2006).

- Roy, S., Benjamin, M.: Modeling of permeation and damage in graphite/epoxy laminates for cryogenic fuel storage. *Composites Science and Technology* **64**(13–14), 2051–2065 (2004).
- Roy, S., Xu, W.: Modeling of diffusion in the presence of damage in polymer matrix composites. *International Journal of Solids and Structures* **38**(1), 115–125 (2001).
- Sadd, M., Parameswaran, D., Shukla, A.: Simulation of asphalt materials using finite element micromechanical model with damage mechanics. *Transportation Research Record* **1832**, 86–95 (2004).
- Schapery, R.: On the characterization of nonlinear viscoelastic materials. *Polymer Engineering and Science* **9**(4), 295–310 (1969).
- Schapery, R.: Nonlinear viscoelastic and viscoplastic constitutive equations with growing damage. *International Journal of Fracture* **97**, 33–66 (1999).
- Seibi, A.C., Sharma, M.G., Ali, G.A., Kenis, W.J.: Constitutive relations for asphalt concrete under high rates of loading. *Transportation Research Record* **1767**, 111–119 (2001).
- Sides, A., Uzan, J., Perl, M.: A comprehensive visco-elastoplastic characterization of sand-asphalt under compression and tension cyclic loading. *Journal of Testing and Evaluation* **13**, 49–59 (1985).
- Simo, J., Hughes, T.: *Computational Inelasticity*, vol. 7. Springer (1998).
- Sousa, J.B., Weissman, S., Sackman, J., Monismith, C.L.: A nonlinear elastic viscous with damage model to predict permanent deformation of asphalt concrete mixtures. *Transportation Research Record* **1384**, 80–93 (1993).
- Sousa, J.B., Weissman, S., Sackman, J., Monismith, C.L.: Modeling permanent deformation of asphalt concrete mixtures. *Journal of the Association of Asphalt Paving Technologists* **63**, 224–257 (1994).
- Tang, X., Whitcomb, J., Li, Y., Sue, H.J.: Micromechanics modeling of moisture diffusion in woven composites. *Composites Science and Technology* **65**(6), 817–826 (2005).
- Tashman, L.: Microstructure viscoplastic continuum model for permanent deformation in asphalt pavements. PhD dissertation, Texas A&M University, College Station, Texas (2003).
- Uzan, J.: Viscoelastic–viscoplastic model with damage for asphalt concrete. *Journal of Materials in Civil Engineering* **17**(5), 528–534 (2005). DOI 10.1061/(ASCE)0899-1561(2005)17:5(528)

- Voyiadjis, G., Abu Al-Rub, R., Palazotto, A.: Thermodynamic formulations for non-local coupling of viscoplasticity and anisotropic viscodamage for dynamic localization problems using gradient theory. *International Journal of Plasticity* **20**(6), 971–1038 (2004).
- Voyiadjis, G., Kattan, P.: *Advances in Damage Mechanics: Metals and Metals Matrix Composites*. Elsevier, Oxford (1999).
- Zollinger, C.: Application of surface energy measurements to evaluate moisture susceptibility of asphalt and aggregates. MS thesis, Texas A&M University, College Station, Texas (2005).